

# The coupled effect of tides and stellar winds on the evolution of compact binaries

Serena Repetto<sup>1\*</sup>, Gijs Nelemans<sup>1,2</sup>

<sup>1</sup>Department of Astrophysics/IMAPP, Radboud University Nijmegen, P.O. Box 9010, 6500 GL Nijmegen, The Netherlands

<sup>2</sup>Institute for Astronomy, KU Leuven, Celestijnenlaan 200D, 3001 Leuven, Belgium

Accepted XXX. Received XXX

## ABSTRACT

We follow the evolution of compact binaries under the coupled effect of tides and stellar winds until the onset of Roche-lobe overflow. These binaries contain a compact object (either a black-hole, a neutron-star, or a planet) and a stellar component. We integrate the full set of tidal equations, which are based on Hut’s model for tidal evolution, and we couple them with the angular momentum loss in a stellar wind. Our aim is twofold. Firstly, we wish to highlight some interesting evolutionary outcomes of the coupling. When tides are coupled with a non-massive stellar wind, one interesting outcome is that in certain types of binaries, the stellar spin tends to reach a quasi-equilibrium state, where the effect of tides and wind are counteracting each other. When tides are coupled with a massive wind, we parametrize the evolution in terms of the decoupling radius, at which the wind decouples from the star. Even for small decoupling radii this *wind braking* can drive systems on the main sequence to Roche-lobe overflow that otherwise would fail to do so. Our second aim is to inspect whether simple timescale considerations are a good description of the evolution of the systems. We find that simple timescale considerations, which rely on neglecting the coupling between tides and stellar winds, do not accurately represent the true evolution of compact binaries. The outcome of the coupled evolution of the rotational and orbital elements can strongly differ from simple timescale considerations, as already pointed out by [Barker & Ogilvie 2009](#) in the case of short-period planetary systems.

**Key words:** binaries: general- binaries: close- planetary systems: planet-star interactions- planets and satellites: gaseous planets- stars: magnetic fields- stars: winds

## 1 Introduction

Just like the Earth and the Moon, stars in binaries raise tidal bulges on each other. Tidal interaction is an important ingredient in binary evolution, and, on secular timescales, it can drive the evolution of the system. Tidal interaction between two bodies dissipates energy, and induces exchange of angular momentum between the orbit and the spin of the components. See [Zahn 2008](#) for a recent comprehensive review on tidal theory in binaries.

We study tidal interaction in binaries formed by a stellar component and a companion which can be approximated as a point mass, i.e. neutron star (NS), black-hole (BH) or planet. Unless the spin angular momentum of the stellar component exceeds  $1/3$  of the orbital angular momentum, the binary orbital and rotational elements evolve in time, and the binary is pushed towards the lowest-energy configuration, on a timescale which depends on the strength of the tidal interaction. This configuration corresponds to a stable solution for the evolution ([Alexander 1973](#), [Darwin 1879](#), [Hut 1980](#)). The equilibrium is characterized by circularity, tidal lock-

ing of the two components (synchronization), and alignment of the stellar spin with respect to the orbital spin. However, an equilibrium solution does not exist in case there is a sink of angular momentum in the system. A possible sink is any stellar wind which carries away angular momentum. One type of angular-momentum loss we consider is *magnetic braking* (MB, see [Parker 1958](#), [Weber & Davis 1967](#), [Verbunt & Zwaan 1981](#)), the loss of angular momentum in a magnetic stellar wind from a low-mass star. The stellar wind, being anchored to the magnetic field lines, is forced to corotate out to large stellar radii, causing large amount of angular momentum being lost from the star and consequently from the orbit, thanks to the tidal coupling. Tides, counteracting the effect of magnetic braking, induce a secular spiral-in of the two stars, driving systems- that would otherwise remain detached- to Roche-lobe overflow (RLO).

Tidal evolution is to be considered in all of those systems which acquire a certain degree of eccentricity and/or asynchronism at some point in their evolution. For instance, progenitors of black-hole and neutron-star X-ray binaries, systems containing a star and a planet, or binaries in globular clusters. Tides are also important in one of the possible models for long gamma-ray bursts, in which the black-hole progenitor that undergoes core-collapse is

\* E-mail: s.repetto@astro.ru.nl

required to be a fast rotator. A way of enhancing the rotation of the progenitor is through synchronization with the orbital motion (see for example Church et al. 2012).

The coupling between tides and magnetic braking in the progenitors of black-hole low-mass X-ray binaries (BH-LMXBs) and neutron-star X-ray binaries (NS-LMXBs) has often been neglected in the past; typically, one assumes that the binary rapidly circularizes and synchronizes; once synchronization is achieved, every bit of angular momentum that is lost from the star, is also lost from the orbit. We aim at investigating whether this model is a good description of the evolution of the systems. In order to do so, we numerically integrate the full set of tidal equations, coupled with magnetic braking, until the Roche-lobe overflow configuration. We then compare our results with the estimates provided by the non-coupled method. We do the same for binaries containing a low-mass star with a planetary companion. We will extend our model to binaries where the stellar companion is of high mass, and we will see how the evolutionary equations need to be modified.

The effect of the coupling between tides and magnetic braking on the evolution of short-period extrasolar planetary systems was studied by Barker & Ogilvie 2009 (hereafter, BO2009). They found that neglecting magnetic braking in this type of systems results in a very different outcome of the evolution. And in particular, they concluded that it is essential to consider the coupled evolution of the rotational and orbital elements, a conclusion which was previously pointed-out by Jackson et al. 2008, who also focused on the orbital evolution of planetary systems.

This paper is divided into 6 sections: in section 2 we present our model and we validate our code, in section 3 we show the binaries we study and we make some predictions of the evolution from simple timescale considerations, in section 4 and 5 we show our results, and in section 6 and 7 we discuss our results and we draw our conclusions.

## 2 Model

### 2.1 Tides coupled with Magnetic Braking

Magnetic braking is the loss of angular momentum in the stellar wind of a main-sequence magnetic star. Low-mass stars ( $0.3 \lesssim M_\star \lesssim 1.5 M_\odot$ ) have radiative cores and convective envelopes, where magnetic fields are thought to be amplified by dynamo processes. Thanks to the corotation of the magnetic field lines out to large distances from the star, any stellar wind takes away large amounts of angular momentum, even if the mass-loss is negligible. The braking is responsible for the slow rotation of most cool and old stars, like the Sun. From Skumanich's empirical law (Skumanich 1972) that describes the dependence of the equatorial velocity on age for main-sequence G stars, the spin-down is obtained as:

$$\frac{d\omega_\star}{dt} = -\gamma_{\text{MB}} R_\star^2 \omega_\star^3 \quad (1)$$

where  $\gamma_{\text{MB}}$  is measured as  $\approx 5 \times 10^{-29} \text{ s/cm}^2$ ,  $R_\star$  is the radius of the star, and  $\omega_\star$  its spin frequency. For the radius of the star, we use the mass-radius relation of a ZAMS-star as in Tout et al. 1996. (Note that the star can grow by up to a factor of 2 on the main sequence). For a review on the different prescriptions of magnetic braking see Knigge et al. 2011.

The star is doomed to lose its rotation within its MS-lifetime,

unless it is tidally coupled to a companion: the rotational angular momentum reservoir of the star is constantly being refueled by the tidal torque.

We follow the Hut 1981 description of tidal interaction, in which tides have small deviations in magnitude and direction from their equilibrium shape, and where dynamical effects are neglected. In this model, the deviation of tides in magnitude and direction is parametrized in terms of a constant and small time-lag  $\tau$ . Orbital elements can therefore be assumed to vary slowly within an orbital period, and their change can be computed through averages along the orbit of the tidal potential.

We extend Hut's equations, valid in the small-angle approximation, to arbitrary inclinations of the stellar spin with the orbital spin, using the same orbit-averaged approach. We note that the tidal model by Hut 1981 was first extended to the case of arbitrary inclinations by Eggleton et al. 1998.

Taking a binary with semi-major axis  $a$ , spin frequency of the star  $\omega_\star$ , eccentricity  $e$ , and inclination of the rotational angular momentum with respect to the orbital angular momentum  $i$ , we write the tidal equations for the evolution of the rotational and orbital elements, adding the magnetic braking term of equation 1:

$$\frac{da}{dt} = -6 \left( \frac{K}{T} \right)_i q(1+q) \left( \frac{R_\star}{a} \right)^8 \frac{a}{(1-e^2)^{15/2}} \left[ f_1(e^2) - (1-e^2)^{3/2} f_2(e^2) \frac{\omega_\star \cos i}{\omega_{\text{orb}}} \right] \quad (2)$$

$$\frac{de}{dt} = -27 \left( \frac{K}{T} \right)_i q(1+q) \left( \frac{R_\star}{a} \right)^8 \frac{e}{(1-e^2)^{13/2}} \left[ f_3(e^2) - \frac{11}{8} (1-e^2)^{3/2} f_4(e^2) \frac{\omega_\star \cos i}{\omega_{\text{orb}}} \right] \quad (3)$$

$$\frac{d\omega_\star}{dt} = 3 \left( \frac{K}{T} \right)_i \frac{q^2}{k^2} \left( \frac{R_\star}{a} \right)^6 \frac{\omega_{\text{orb}}}{(1-e^2)^6} \left[ f_2(e^2) \cos i - \frac{1}{4} \frac{\omega_\star}{\omega_{\text{orb}}} (1-e^2)^{3/2} (3 + \cos 2i) f_5(e^2) \right] - \gamma_{\text{MB}} R_\star^2 \omega_\star^3 \quad (4)$$

$$\frac{di}{dt} = -3 \left( \frac{K}{T} \right)_i \frac{q^2}{k^2} \left( \frac{R_\star}{a} \right)^6 \frac{\sin i}{(1-e^2)^6} \frac{\omega_{\text{orb}}}{\omega_\star} \left[ f_2(e^2) - \frac{f_5(e^2)}{2} \right] \times \left( \frac{\omega_\star \cos i (1-e^2)^{3/2}}{\omega_{\text{orb}}} + \frac{R_\star^2 a \omega_\star^2 k^2 (1-e^2)}{M_{\text{comp}} G} \right) \quad (5)$$

where  $M_{\text{comp}}$  is the mass of the compact companion,  $M_\star$  the mass of the star,  $q$  the mass-ratio  $M_{\text{comp}}/M_\star$ , and the functions  $f_i(e^2)$  are polynomials in  $e^2$  as in Hut 1981. For the radius of gyration  $k$ , we use the fitting formula given in de Mink et al. 2013, which is based on the detailed stellar evolution models of Pols et al. 1998, and which gives the mass-dependence of  $k$ .

The calibration factors  $\{K/T\}_{i=c,r}$  measure the strength of the dissipation of the tidal flow.  $K$  is the apsidal motion constant, which takes into account the central condensation of the star (Lecar et al. 1976).  $T$  is a typical timescale on which significant changes in the orbit take place through tidal evolution; in units of the orbital period,  $T$  is the inverse of the tidal time-lag  $\tau$ . In his derivation, Hut considers a constant time-lag  $\tau$ . However, it has been later argued whether this was the appropriate choice. The time-lag should in fact be compared with typical relaxation time of the process responsible for the dissipation. The source of dissipation depends

on the type of star which undergoes tidal deformations (see Zahn 1977).

Low mass stars have convective envelopes and it is believed that turbulent convection is responsible for the dissipation. When viscosity results from turbulence, the natural relaxation time is the eddy-turnover timescale  $\tau_{\text{conv}}$ . This may be longer than the orbital period, in which case the efficiency of the dissipation should be reduced. The efficiency should then be dependent on the tidal forcing frequency (see Goldreich & Nicholson 1977, Zahn 1989, Ivanov & Papaloizou 2004).

Two scalings have been proposed for the viscosity due to the turbulent convection. Zahn 1966 assumes a linear scaling with the tidal forcing frequency. He expresses  $f_{\text{conv}}$ , the fraction of the convective cells which contribute to the damping, as:

$$f_{\text{conv}} = \min \left[ 1, \left( \frac{P_{\text{tid}}}{2\tau_{\text{conv}}} \right) \right] \quad (6)$$

where  $P_{\text{tid}}$  is the tidal forcing period, given by:

$$\frac{1}{P_{\text{tid}}} = \left| \frac{1}{P_{\text{orb}}} - \frac{1}{P_{\star}} \right| \quad (7)$$

For high tidal-forcing frequency (i.e. when  $P_{\text{tid}} \ll \tau_{\text{conv}}$ ) the efficiency of momentum transfer by the largest convective cells is reduced. Instead, Goldreich & Nicholson 1977 suggested a quadratic dependence:

$$f_{\text{conv}} = \min \left[ 1, \left( \frac{P_{\text{tid}}}{2\tau_{\text{conv}}} \right)^2 \right] \quad (8)$$

There is a long-standing uncertainty regarding which scaling is correct, with some numerical simulations of turbulent viscosity in a convection zone favoring a linear scaling (Penev et al. 2007), while others favoring a quadratic scaling (Ogilvie & Lesur 2012).

The question of tidal dissipation in a convective shell is still ‘‘Achille’s heel of tidal theory’’, as Zahn 2008 wrote, and it goes beyond the scope of this Paper. We choose  $f_{\text{conv}}$  as in eq. 8. In this we follow the approach by Hurley et al. 2002, Belczynski et al. 2008 and Valsecchi & Rasio 2014, who express the calibration factor for a convective envelope as:

$$\left( \frac{K}{T} \right)_c = \frac{2}{21} \frac{f_{\text{conv}}}{\tau_{\text{conv}}} \frac{M_{\text{env}}}{M_{\star}} [\text{yr}^{-1}] \quad (9)$$

where  $M_{\text{env}}$  is the mass in the convective envelope.

Zahn’s prescription seem to be in better in agreement with observations of tidal circularization times for binaries containing a giant star (Verbunt & Phinney 1995). A more recent work by Belczynski et al. 2008, showed the need for multiplying  $f_{\text{conv}}$  in eq. 8 by 50, to match the observed circularization period of close binary stars. However, due to general uncertainties on tidal calibration for a convective envelope, we find our model a reasonable place to start.

Another uncertainty is whether and how the time-lag should depend on the misalignment between the stellar spin and the orbital angular momentum. There is not yet agreement on this (Adrian Barker, priv. communication), and we prefer not to add additional parameters to our model.

High-mass stars have radiative envelopes, and tidal motions are assumed to be dissipated via radiative damping of the stellar  $g$ -modes. In this case the calibration factor is (Hurley et al. 2002, Belczynski et al. 2008):

$$\left( \frac{K}{T} \right)_r = 1.9782 \times 10^4 \frac{M_{\star} R_{\star}^2}{a^5} (1 + q)^{5/6} E_2 [\text{yr}^{-1}] \quad (10)$$

where  $E_2$  is a second-order parameter which measures the coupling between the tidal potential and the gravity mode (Zahn 1975); we fit it to the values given by Zahn 1975:

$$E_2 = 1.58313 \times 10^{-9} M_{\star}^{2.84} \quad (11)$$

(see also Hurley et al. 2002).

## 2.2 Non-coupled methods

One way of following the evolution of a binary system in which tidal friction and magnetic braking are both operating, is to assume synchronization and to circularize the binary instantaneously or on a certain circularization timescale, neglecting the spin of the star. The new semi-major axis is then  $a_{\text{circ}} = a(1 - e^2)$ . This choice appears reasonable when dealing with systems in which the angular momentum stored in the tidally-deformed component is small (i.e. the moment of inertia of the star is small). Tidal interaction conserves the total angular momentum  $J_{\text{tot}} = J_{\text{orb}} + J_{\star}$ . Neglecting  $J_{\star}$ , conservation of  $J_{\text{orb}}$  gives  $a_{\text{circ}} = a(1 - e^2)$ . Afterwards, the tidal torque counteracts the effect of the magnetic spin-down, bringing angular momentum from the orbit back into the star. It is then reasonable to assume that every bit of angular momentum which is lost from the star, is also lost from the orbit (i.e.  $\dot{J}_{\text{orb}} = \dot{J}_{\star}$ , see Verbunt & Zwaan 1981). The rate of angular momentum loss in the stellar wind is:

$$\frac{dJ_{\star}}{dt} = k^2 M_2 R_{\star}^2 \frac{d\omega_{\star}}{dt} \quad (12)$$

where we have neglected the change in radius and mass of the star, for the mass-loss being negligible (typically,  $|\dot{M}_{\star}| \sim 10^{-14} M_{\odot} / \text{yr}$  for a Sun-like star). Using  $\dot{a}/a = 2\dot{J}_{\text{orb}}/J_{\text{orb}} = 2\dot{J}_{\star}/J_{\text{orb}}$  and equation 1, and assuming  $\omega_{\star} = \omega_{\text{orb}}$ , the semi-major axis decay rate is:

$$\frac{da}{dt} = - \frac{2\gamma_{\text{MB}} k^2 R_{\star}^4 G M^2}{M_{\text{comp}}} \frac{1}{a^4} \quad (13)$$

where  $M$  is the total mass of the binary. We will call this approach *non-coupled* method.

Our approach instead is to numerically-integrate the full set of tidal equations coupled with the magnetic spin-down (eqs. 2-3-4-5). In section 4 we present the results of this integration for some illustrative binaries, showing how they differ from the results in the non-coupled method. A particular stress will be given to circularization timescales. Some previous works used these timescales as a simple way of depicting the evolution of compact binaries. It turns out that the true evolution of the eccentricity can highly differ from the exponential decay implied by the choice of a circularization timescale as  $e/\dot{e}$ .

## 2.3 Validation of the evolution code

For small values of the inclination, our tidal equations for an eccentric and non-coplanar binary recover the equations in Hut 1981. In contrast to the BO2009 equations, we write down explicitly the tidal equations for  $(a, e, \omega_{\star}, i)$  in the case of a non-circular and non-coplanar orbit. BO2009 choose instead of constant time-lag  $\tau$  like in Hut’s model, a constant  $Q'$ , where  $Q'$  is a re-parametrization of the tidal calibration factor  $Q$ . The factor  $Q$ , also called *quality factor*, is a dimensionless quantity used mainly in planetary studies for characterizing the efficiency of tidal dissipation. BO2009 take  $Q' = 10^6$  (see also Ogilvie & Lin 2007). We recover the equations 4, 5, 6 in BO2009 for a circular and non-coplanar orbit, when replacing  $K/T$  in our equations with  $\frac{3}{2Q'} \frac{1}{\omega_{\text{orb}}} \frac{GM_{\star}}{R_{\star}^3}$ .

In order to validate our code, we reproduce some of the results presented by BO2009. Figure 1 is a phase-portrait plot, showing the evolution in the plane  $(\tilde{n}, \tilde{\Omega})$  of coplanar and circular systems with varying initial conditions. The variables  $\tilde{n}$  and  $\tilde{\Omega}$  are reparametrization of the orbital frequency and the stellar spin frequency respectively, which have been normalized to the orbital frequency at the stellar surface, together with a constant factor (see BO2009 for details). In integrating our evolutionary equations, we have replaced our tidal calibration factor  $K/T$  with  $\frac{3}{2Q'} \frac{1}{\omega_{\text{orb}}} \frac{GM_*}{R_*^3}$ , and we have used BO2009 calibration for magnetic braking ( $\gamma_{\text{MB}}$  in our model is 0.4 times smaller than  $\gamma_{\text{MB}}$  in BO2009). Figure 1 coincides with the top plot in fig.1 of BO2009. Once magnetic braking spins down the star below corotation ( $\tilde{\Omega} < \tilde{n}$ ) the orbit undergoes tidally-induced decay.

We also integrate our evolutionary equations for a set of planetary systems with circular and non-coplanar orbit ( $i = 90^\circ$ ), and we show the corresponding solutions in the phase-portrait plot of figure 2. The overall evolution is similar to the one in figure 1, the only difference being that system with  $\tilde{\Omega} \cos i < \tilde{n}$  undergo orbital decay while still being outside corotation. This plot is identical to the top plot in fig.3 in BO2009.

### 3 Binaries in our study

We present the binaries we consider in our study in figure 3. The most extreme ones are binaries in which the magnetic wind from a low-mass star is coupled with the tidal friction between the star and its compact companion. The companion is either a black-hole, or a Hot Jupiter, which is a planet with mass similar to Jupiter at a distance less than 0.1 AU from its host star.

We will also extend our model to a case in which the star is of high-mass instead (see section 5). The companion is either a neutron star, a black-hole, or, in a more exotic scenario, a white dwarf (WD).

Together these systems span a wide range of mass ratios, ranging from  $q = 0.001 - 10$ .

We will refer to a binary containing a black hole or a neutron star as a black-hole X-ray binary of high or low mass (BH-HMXB/BH-LMXB), or a neutron-star high/low-mass X-ray binary (NS-HMXB/NS-LMXB), where low and high refer to the mass of the companion. We point out though that these terms commonly refer to the mass-transfer phase, which is one of the evolutionary stages experienced by these binaries. What we deal with instead are systems on their way of becoming X-ray binaries, that is, we study the secular phase before mass-transfer sets in.

#### 3.1 Timescale considerations

Before going into the details of the numerical integration of the coupled equations 2-3-4-5, we wish to make some predictions on the evolution of the systems based on simple timescale considerations<sup>†</sup>.

The binaries in our study are presented in figure 3 in terms of their mass-ratio  $q$  and the ratio  $\eta = J_*/J_{\text{orb}}$ .  $J_{\text{orb}}$  is calculated for a circular orbit with  $a = 2 a_{\text{RLO}}$ .  $a_{\text{RLO}}$  is the orbital separation at

<sup>†</sup> As a note, throughout the paper we will indicate the timescale of a certain event with  $\tau$ , whereas  $t$  will indicate the time of occurrence of the same event in our integration.

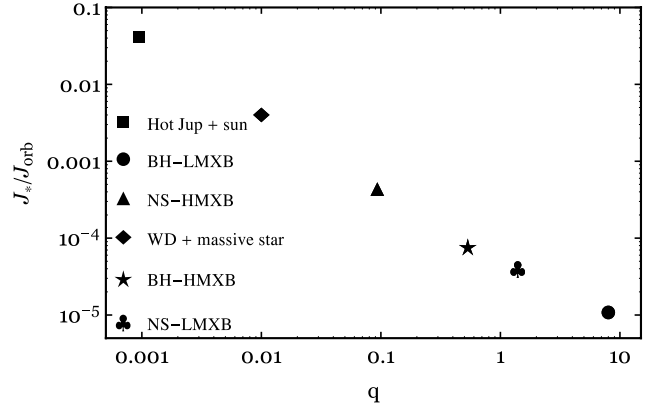


**Figure 3.** Different types of compact binaries as a function of the ratio  $J_*/J_{\text{orb}}$  between the rotational and the orbital angular momentum and as a function of the binary mass ratio  $q$ .

which the system undergoes RLO, i.e.  $a_{\text{RLO}} = R_*/f(1/q)$ , where  $f(q)$  is a function of the mass-ratio as in Eggleton 1983.  $J_*$  is calculated for a slow-spinning star with  $\omega_* = 10^{-3} \omega_{\text{break}}$ , where  $\omega_{\text{break}}$  is the break-up frequency  $\sqrt{GM_*/R_*^3}$ . The ratio  $\eta$  is then larger for faster-spinning star. It is an indicator for how much angular momentum is stored in the star compared to how much is stored in the orbit. A larger  $\eta$ , like in the planetary system case, implies that tides will more easily bring changes to the orbit than to the spin. If the orbit is sufficiently close, the planetary system suffers a significant tidal decay, while the tidal change of the stellar spin is much less significant. The opposite happens in a BH-LMXB, where tides easily affect the stellar spin.

The larger the mass-ratio, the smaller the timescale on which tides cause significant changes to the orbital and rotational elements, as can be seen from the dependence on the mass-ratio of the tidal equations 2-3-4-5. Hence tides are much more efficient in a BH-LMXB than in a planetary system.

We can obtain a rule of thumb for determining which systems will first circularize rather than synchronize. The circularization timescale can be estimated as  $e/\dot{e}$  where  $\dot{e}$  is as in equation 3, and assuming  $e \approx 0$  and  $\omega_* = \omega_{\text{orb}}$  (Hurley et al. 2002):

$$\frac{1}{\tau_{\text{circ}}} = \frac{21}{2} \left( \frac{K}{T} \right)_c q (1+q) \left( \frac{R_*}{a} \right)^8 \quad (14)$$

The synchronization timescale for a circular orbit is calculated as (Hurley et al. 2002):

$$\frac{1}{\tau_{\text{sync}}} = \left| \frac{\dot{\omega}_*|_{\text{tid}}}{\omega_* - \omega_{\text{orb}}} \right| = 3 \left( \frac{K}{T} \right) \frac{q^2}{k^2} \left( \frac{R_*}{a} \right)^6 \quad (15)$$

Then  $\tau_{\text{circ}} < \tau_{\text{sync}}$  when:

$$\frac{kR_*}{a} > \sqrt{\frac{6}{21} \frac{q}{1+q}} \quad (16)$$

where the star can be modeled as a rigid sphere of radius  $kR_*$ . Taking  $a = 2 a_{\text{RLO}}$ , the criteria is satisfied for two of the types of binaries we showed in figure 3: the planetary system and the binary consisting of a white-dwarf and a massive star. In all the other cases, we expect the first phase of the evolution of the binary to be driven by changes in the stellar spin rather than the orbit.

In our model the spin is being affected both by tides and by magnetic braking; we compare their typical timescales.



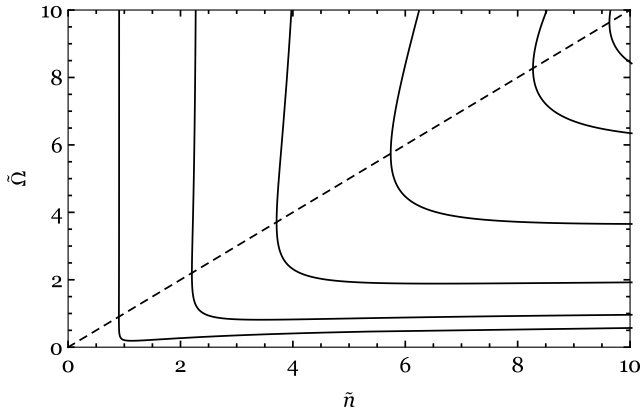


**Figure 1.** Evolution of a coplanar and circular planetary system with varying initial conditions in the plane ( $\tilde{n}$ ,  $\tilde{\Omega}$ ) (solid lines). The diagonal line corresponds to corotation  $\tilde{\Omega} = \tilde{n}$ .

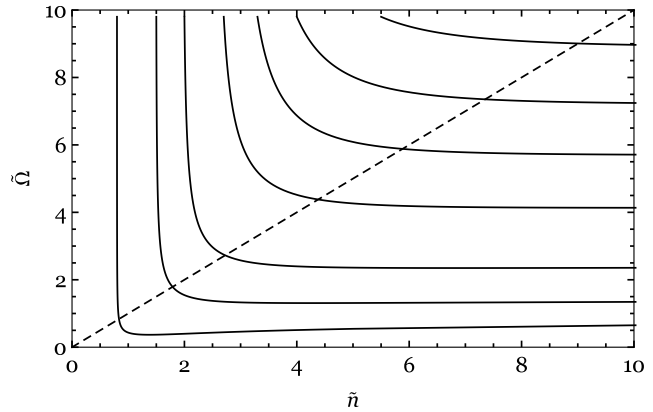


**Figure 2.** Evolution of a circular and non-coplanar ( $i = 90^\circ$ ) planetary system with varying initial conditions in the plane ( $\tilde{n}$ ,  $\tilde{\Omega}$ ) (solid lines). The diagonal line corresponds to corotation  $\tilde{\Omega} = \tilde{n}$ .

The MB spin-down timescale is calculated as:

$$\frac{1}{\tau_{\text{MB}}} = \frac{\dot{\omega}_{\star|\text{MB}}}{\omega_{\star}} \quad (17)$$

where  $\dot{\omega}_{\star|\text{MB}}$  is as in equation 1. In figure 4, we show the synchronization timescale and the circularization timescale for a binary composed of a low-mass star ( $M_{\star} = 1 M_{\odot}$ ), as a function of the compact companion mass (solid black and solid gray line). Timescales are calculated using equations 14 and 15. The orbital separation is taken to be  $a = 2 a_{\text{RLO}}$  and the star is spinning with  $\omega = 0.9 \omega_{\text{break}}$ . We also show the MS-lifetime, the MB spin-down timescale for a star spinning at  $0.9 \omega_{\text{break}}$ , the MB spin-down timescale for a star spinning at  $\omega_{\text{eq}}$ , and for a star spinning at  $10^{-5} \omega_{\text{break}}$ .

The quasi-equilibrium frequency  $\omega_{\text{eq}}$  is the frequency at which MB and tidal torque are balancing each other (i.e.  $|\dot{\omega}_{\star, \text{MB}}| = |\dot{\omega}_{\star, \text{tid}}|$ , see section 4 for further details). It has been calculated for an orbit with  $a = 2 a_{\text{RLO}}$  and  $e = 0.1$ .

For low mass-ratios, tides are weak. Consequently, magnetic braking spins-down the star below corotation ( $\omega_{\star} < \omega_{\text{orb}}$ ), and tides won't manage to synchronize the spin frequency to the orbital frequency within a MS-lifetime. This is what happens in the planetary-system case. Instead, in a BH-LMXB tides and magnetic braking tend to reach a quasi-equilibrium state in which they balance each other.

Concerning the circularization timescale, it is typically shorter than the synchronization timescale for  $q < 0.05$ , like in the planetary system case.

When tides and magnetic braking are coupled, we can use this figure to predict the evolution of the binary. If a star is initially spinning at  $0.9 \omega_{\text{break}}$ ,  $\tau_{\text{MB}}$  is shorter than  $\tau_{\text{sync}}$ . This means that in the first phase of the evolution MB spins down the star, until the timescale on which tides act on the spin becomes comparable to the MB timescale, and tides start playing a role.

## 4 Results

### 4.1 Black-hole low-mass X-ray binary

The orbit of a black-hole low-mass X-ray binary is typically eccentric right after the formation of the black-hole. The eccentricity is the result of the mass ejection and/or possibly the natal kick

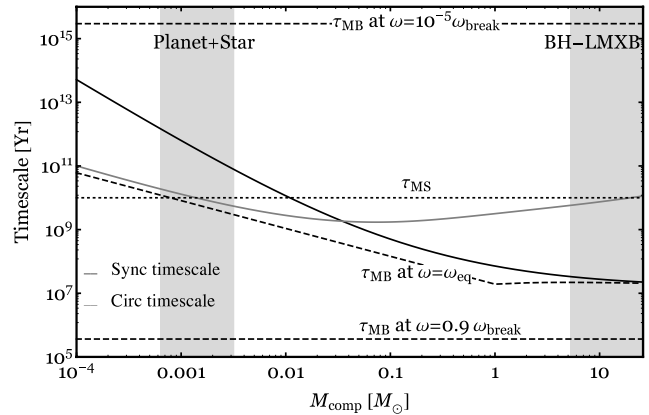


**Figure 4.** The solid black line and the solid gray line show respectively the synchronization and circularization timescale for a binary with  $a = 2 a_{\text{RLO}}$  composed of a sun-like star and a companion of mass  $M_{\text{comp}}$ . The dotted line shows the MS-lifetime, whereas the dashed lines show the MB spin-down timescale for  $\omega_{\star} = 0.9 \omega_{\text{break}}$ , the MB spin-down timescale for  $\omega_{\star} = \omega_{\text{eq}}$  (see text for details on  $\omega_{\text{eq}}$ ), and for  $\omega_{\star} = 10^{-5} \omega_{\text{break}}$ .

in the supernova which gives birth to the black hole. In addition, any component of the natal kick perpendicular to the orbital plane will result in a misalignment between the orbital spin and the stellar spin. The most effective way of shrinking a BH-LMXB down to the RLO configuration is a coupling between the magnetic wind from the low-mass star and tidal friction, whereas gravitational wave emission can be neglected for the typical initial orbital separations ( $a \approx 10 R_{\odot}$ ).

Previous binary population synthesis (BPS) works on the evolution of BH-LMXBs have neglected the coupling between the stellar spin and the orbital spin, following the evolution of the binaries according to what we call the non-coupled method (see for example Kalogera 1999 and Yungelson et al. 2006). This has been done for NS-LMXBs too, see for example Pylyser & Savonije 1988 and Ma & Li 2009. This choice was motivated by the fact that the rotational angular momentum is small compared to the orbital angular momentum. Also, the tidal evolution of the misalignment between the spin of the star and the orbital spin has usually been neglected.

#### 4.1.1 An illustrative example of the evolution in the coplanar case

We integrate the tidal equations 2, 3, 4, 5 for an illustrative system formed by a black hole of mass  $M_{\text{BH}} = 8 M_{\odot}$  and a star of mass  $M_{\star} = 1 M_{\odot}$ , until the RLO configuration is reached ( $a_{\text{RLO}} \approx 4 R_{\odot}$ ). The rotational angular momentum is small compared to the orbital one (see figure 3), thus we expect the system to rapidly reach the synchronous state.

In figure 5 we show the evolution for initial orbital parameters  $a = 22 R_{\odot}$ ,  $e = 0.7$  and  $i = 0$ . Concerning the spin of the star, we consider both a star spinning at  $\omega_{\star} = 0.9 \omega_{\text{break}}$  (see solid thick lines), and at  $\omega_{\star} = 10^{-5} \omega_{\text{break}}$  (dashed thick lines).

Either via magnetic spin-down (high-spin case) or via tidal spin-up (low-spin case), the spin frequency converges to  $\omega_{\text{eq}}$ , where  $\omega_{\text{eq}}$  is the spin-frequency such that  $|\dot{\omega}_{\star, \text{MB}}| = |\dot{\omega}_{\star, \text{tid}}|$  (plateau in the left panel in figure 5). The approach of this *quasi-equilibrium* state  $\ddagger$  is allowed by the fact that both  $\dot{\omega}_{\star, \text{MB}}$  and  $\dot{\omega}_{\star, \text{tid}}$  depend on the stellar spin (see equations 1 and 4).

Both solutions reach the quasi-equilibrium state  $\omega_{\text{eq}}$  on a similar timescale, which is very short ( $\approx 10^{-3} t_{\text{MS}}$ ), therefore no significant changes in the orbit take place during this phase. Afterwards, the orbit circularizes and the spin synchronizes to the orbital frequency. We note that the time for the orbit to become circular is non-negligible ( $t_{\text{circ}} \sim 6 \times 10^{-2} t_{\text{MS}}$ ). Once synchronization and circularization are achieved, every bit of angular momentum which is lost from the star in the wind, is also lost from the orbit. The two components effectively approach each other until RLO, and equation 13 describes well the evolution of the system. During this phase of the evolution, tides and magnetic braking are perfectly counteracting each-other, i.e.  $\dot{\omega}_{\star}|_{\text{MB}} = \dot{\omega}_{\star}|_{\text{tid}}$ .

#### 4.1.2 Comparison with non-coupled methods

We also compare the results of our integration with the estimates of the non-coupled method, both for the low-spinning case and the high-spinning case. The results are presented in the center panel of figure 5, where we show the evolution of the semi-major axis in the non-coupled method. We take two types of circularization timescale; one as in equation 14 (dark gray lines), and one given by  $\tau_{\text{circ}} = e/\dot{e}$  (light gray lines). Solid lines are for the high spinning case and dashed lines for the low spinning case. The circularized orbital separation is overestimated in both scenarios, since changes in the orbit once the binary reaches the quasi-equilibrium state, are neglected in non-coupled methods. As a consequence, the age of the binary at the RLO configuration is overestimated. When taking  $\tau_{\text{circ}} = e/\dot{e}$ , it is overestimated by a factor of  $\approx 2.6$  in the high-spin case, and by  $\approx 1.3$  in the low-spin case. The time it takes to reach circularization in our integration is  $t_{\text{circ}} \approx 0.06 t_{\text{MS}}$ . The ratio  $t_{\text{circ}}/\tau_{\text{circ}}$  when taking  $\tau_{\text{circ}} = e/\dot{e}$ , is 0.05 in the high-spin case, and 20 in the low-spinning case. With  $\tau_{\text{circ}}$  as in equation 14, the ratio is  $2 \times 10^{-5}$  and 0.03 respectively.

A better estimate of the time it takes to reach circularization would arise taking a star spinning at half the break-frequency in the calculation of  $e/\dot{e}$  (see for details figure 7).

This illustrative example highlights the importance, at least in the first phase of the evolution (before circularization is achieved), of considering the coupled evolution of the rotational and orbital element.

$\ddagger$  We call it *quasi-equilibrium* state due to the fact that the orbital properties are still evolving.

#### 4.1.3 An illustrative example of the evolution in the misaligned case

Misalignment has usually been neglected, and we wonder whether it brings significant changes to the orbital evolution. Due to the small angular momentum stored in the star ( $J_{\star}/J_{\text{orb}} \ll 1$ ), we expect the tidal torque to easily affect  $J_{\star}$ . That is, we expect the stellar spin to rapidly align and synchronize with the orbital spin.

In figure 6 we show a representative illustration of the evolution of a BH-LMXB with initial orbital parameters  $a = 9 R_{\odot}$ ,  $e = 0.5$ , with the star in a retrograde orbit around the black hole ( $i = 120^{\circ}$ ) and spinning at  $0.9 \omega_{\text{break}}$ . Once magnetic braking has spun-down the star sufficiently, the spin aligns with the orbital angular momentum. This can be seen in the right panel in the figure, which shows how steeply the inclination decreases once the spin of the star has become negligible. An interesting difference with respect to the evolution in the coplanar case, is the initial decay of the orbital separation of a retrograde orbit. This is due to the fact that  $\omega_{\star} \cos i < \omega_{\text{orb}}$ . In the retrograde case, or in any case when the previous condition is satisfied, there is a first phase in which tides and magnetic braking are simultaneously at work. In the coplanar case, instead, the first phase of the evolution is dominated either by tides or by magnetic braking, that act in opposite directions.

In case magnetic braking is not present, the star would align, but on a longer timescale. This is due to the fact that magnetic braking is much more efficient than tides in spinning down the initially high-spinning star. Once the star has been spun-down, the spin rapidly aligns. For the binary configuration we've just showed the ratio between the time at which the spin aligns in the magnetic braking case and in the tides-only case is  $\approx 0.6$ .

#### 4.1.4 Population study

As a more general diagnostic of the discrepancy between the coupled and the non-coupled method, we now do a population study, investigating how both the orbital separation at the time the binary circularizes and the time it takes to reach circularization, change over the population. In the non coupled method, the two quantities just mentioned are given by  $a_{\text{circ}} = a(1 - e^2)$  and  $\tau_{\text{circ}} = e/\dot{e}$ .

The initial values  $e_0$  of the eccentricity are taken from a grid which spans the interval  $[0.001, 0.901]$ . For each value of the eccentricity, we draw uniform values  $a_0$  for the orbital separation in the interval  $[a_{\text{min}}(e), a_{\text{max}}(e)]$ .  $a_{\text{min}}(e) = a_{\text{RLO}}/(1 - e)$  is the orbital separation at which the system undergoes RLO at periastron;  $a_{\text{max}}(e)$  is the maximal orbital separation such that the system undergoes RLO within the MS-lifetime. We draw uniform values  $\omega_{\star, 0}$  for the stellar spin in the interval  $[0, \omega_{\text{break}}]$ , and uniform values  $i_0$  in  $[0^{\circ}, 180^{\circ}]$ .

For each initial condition  $(a_0, e_0, \omega_{\star, 0}, i_0)$ , we integrate the tidal equations coupled with magnetic braking and we study the properties of 1000 solutions which undergo RLO within the MS-lifetime. We calculate the ratio between the value in the coupled method and the value in the non-coupled method of the previously mentioned variables as a function of the eccentricity. We show the results in figure 11 and figure 7.

For each value of the eccentricity there is a range of values for  $t_{\text{circ}}/\tau_{\text{circ}}$ . The spread in the values at a fixed eccentricity is mainly caused by different initial spin frequencies. This was already seen in figure 5, where taking either a low-spinning star or a high spinning star, under-estimates or over-estimates  $t_{\text{circ}}$ .

To show how the spread in the ratio  $t_{\text{circ}}/\tau_{\text{circ}}$  is reduced when

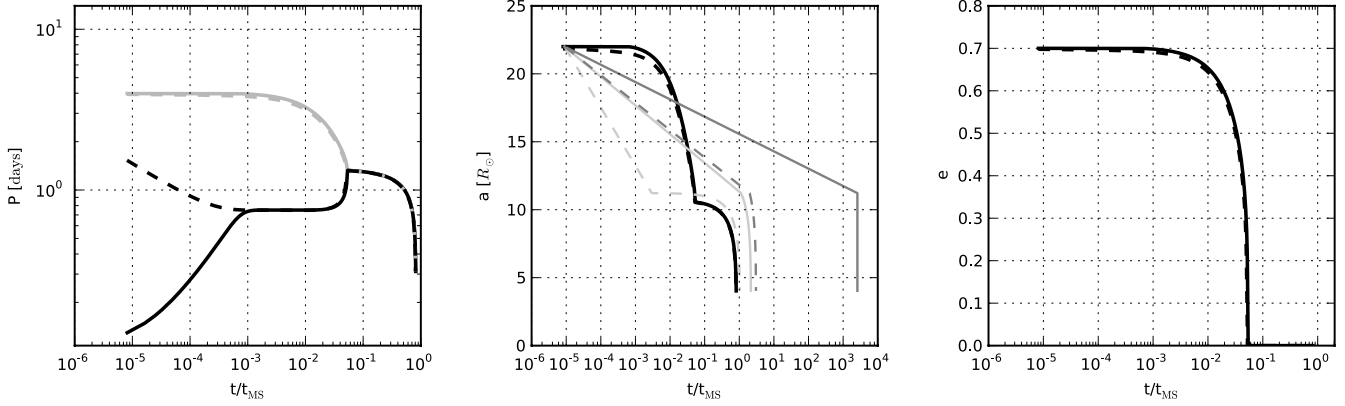


**Figure 5.** Evolution of a coplanar and eccentric BH-LMXB under the effect of tides and magnetic braking. The binary is composed of a black-hole of mass  $8 M_{\odot}$  and a one solar-mass star. Initial orbital parameters are  $a = 22 R_{\odot}$ ,  $e = 0.7$ ,  $i = 0$ . We consider both a high-spinning star ( $\omega_{\star} = 0.9 \omega_{\text{break}}$ ) and a low-spinning star ( $\omega_{\star} = 10^{-5} \omega_{\text{break}}$ ). In all the three panels, the solid lines correspond to the high-spin, the dashed lines to low-spin. The left panel shows the evolution of the stellar rotation period in black and of the orbital period in grey. The middle panel shows the evolution of the orbital separation, whereas the right one represents the evolution of the eccentricity. In the center panel, the two thick black lines represent the evolution of the orbital separation in our integration. The thin dark-gray lines represent the evolution of the orbital separation in the non-coupled method when taking  $\tau_{\text{circ}} = (e/\dot{e})|_{e \approx 0, \omega_{\star} = \omega_{\text{orb}}}$ ; thin light-gray lines when taking  $\tau_{\text{circ}} = e/\dot{e}$ .

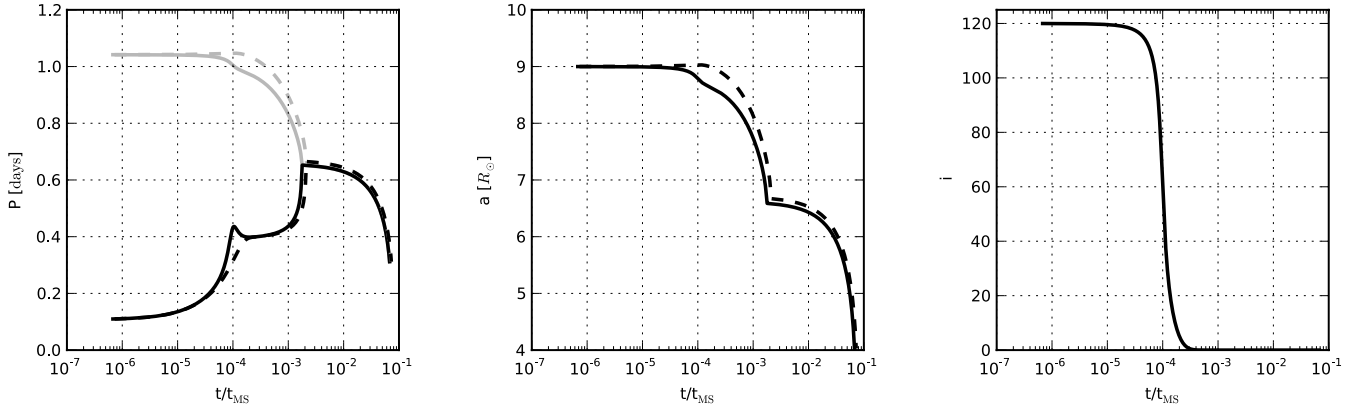


**Figure 6.** Evolution of a misaligned and eccentric BH-LMXB under the effect of tides and magnetic braking. The binary contains a black-hole of mass  $8 M_{\odot}$  and a one solar-mass star. Initial orbital parameters are  $a = 9 R_{\odot}$ ,  $e = 0.5$ ,  $i = 120^{\circ}$ . The left panel show the evolution of the rotation period of the star (black solid line) and of the orbital period (grey solid line). The middle panel shows the evolution of the orbital separation (solid black line). The right panel shows the evolution of the eccentricity (solid black line). The dashed lines in all of the three panels correspond to the evolution of a BH-LMXB with the same initial condition for  $(\omega_{\star}, a, e)$ , but with no misalignment between the spin and the orbit.

fixing the initial spin of the star, we show in figure 7 the ratio  $t_{\text{circ}}/\tau_{\text{circ}}$  when the initial spin is chosen to be  $\omega_{\star} = 1/2 \omega_{\text{break}}$  (dark grey shaded area). When we fix instead the orbital separation at birth (as an example, we take the average value between  $a_{\text{min}}(e)$  and  $a_{\text{max}}(e)$ ), the spread is conserved (light grey shaded area).

We also calculate the ratio  $t_{\text{circ}}/\tau_{\text{circ}}$  when taking for  $\tau_{\text{circ}}$  the expression in equation 14, see figure 8. The decrease in the ratio is caused by the dependence of  $\tau_{\text{circ}}$  on the orbital separation, which increases with increasing eccentricities, and  $\tau_{\text{circ}}$  increases accordingly.

Concerning the ratio between the orbital separation at  $e = 0$  in our integration ( $a_{e=0}$ ) and  $a_{\text{circ}} = a(1 - e^2)$ , it is typically less than 1. This is due to the fact that as soon as magnetic braking has spun-down the star sufficiently, tides start removing angular momentum from the orbit, before synchronization is achieved. This effect is neglected in the non-coupled method. The decrease of the

ratio with the eccentricity, is a consequence of the  $a_{\text{circ}}$  dependence on  $(1 - e^2)$ .

We also calculate the ratio between the time it takes to reach the RLO configuration in our integration ( $t_{\text{RLO}}$ ) and the estimated value for it in the non-coupled method ( $\tau_{\text{RLO}}$ ). In the non-coupled method, we calculate  $\tau_{\text{RLO}}$  in two ways. One as  $\tau_{\text{circ}} + \tau_{\text{VZ}}$ , the other as  $\tau_{\text{VZ}}$ . In the first way we integrate the equation 13 taking as initial condition  $a_{\text{circ}} = a(1 - e^2)$ ; this gives  $t_{\text{VZ}}$ . We then calculate  $\tau_{\text{RLO}}$  as  $\tau_{\text{circ}} + \tau_{\text{VZ}}$ , where  $\tau_{\text{circ}} = e/\dot{e}$ . The other way relies on assuming instantaneous circularization and taking  $\tau_{\text{RLO}} = \tau_{\text{VZ}}$ , where  $\tau_{\text{VZ}}$  is  $a/\dot{a}$  with  $\dot{a}$  as in equation 13, and again we use  $a_{\text{circ}} = a(1 - e^2)$  when calculating  $\tau_{\text{VZ}}$ . This way of estimating  $\tau_{\text{RLO}}$  has been mostly used in previous BPS works on the evolution of binaries hosting a black-hole or a neutron star. We show the respective outcomes in figures 9 and 10. The decrease in the ratio which appears in figure 10 is due to the fact that for higher eccentricities, both  $a_{\text{min}}$  and  $a_{\text{max}}$  increase;  $\tau_{\text{VZ}}$  increases accordingly.

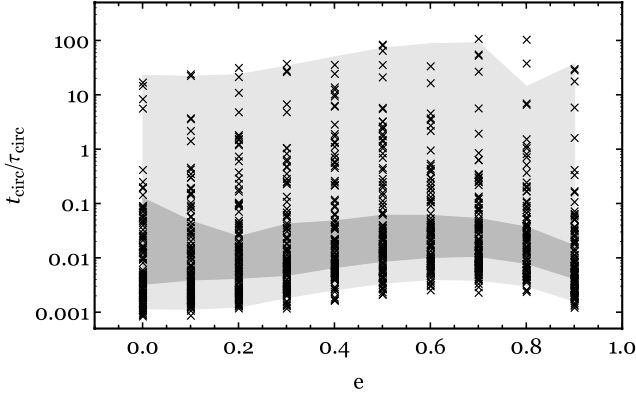


**Figure 7.** Ratio between the time it takes to reach circularization in the coupled and non-coupled method for 1000 black-hole low-mass X-ray binaries undergoing RLO within the MS-lifetime, when taking  $\tau_{\text{circ}} = e/\dot{e}$ . The light grey shaded area is for a fixed initial orbital separation, and the darker grey area is for a fixed initial stellar spin.

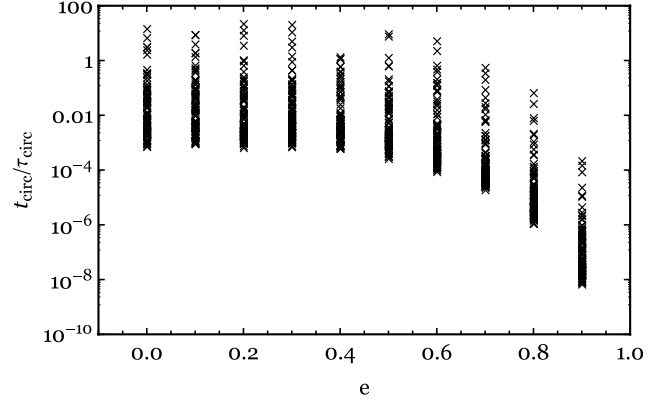


**Figure 8.** Ratio between the time it takes to reach circularization in the coupled and non-coupled method for 1000 black-hole low-mass X-ray binaries undergoing RLO within the MS-lifetime, when taking  $\tau_{\text{circ}}$  as in eq. 14.

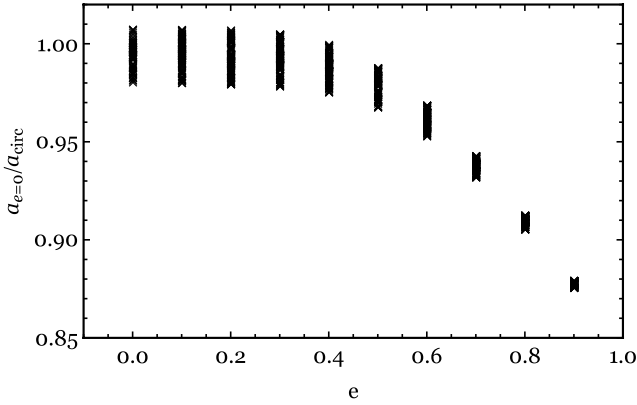


**Figure 11.** Ratio between the orbital separation at  $e = 0$  and  $a_{\text{circ}}$  for 1000 black-hole low-mass X-ray binaries undergoing RLO within the MS-lifetime.

When choosing  $\tau_{\text{RLO}}$  as  $\tau_{\text{circ}} + t_{\text{VZ}}$ , the ratio is constrained to be in the interval  $(0.1 - 1)$ , so we find this way of calculating  $\tau_{\text{RLO}}$  a better estimate than when  $\tau_{\text{RLO}} = \tau_{\text{VZ}}$ .

## 4.2 Planetary system

We follow the evolution of a planetary system as well, composed of a Sun-like star and a Hot Jupiter.

### 4.2.1 An illustrative example of the evolution in the coplanar case

We show an illustration of the evolution until the planet fills its Roche-lobe (at  $a_{\text{RLO}} \approx 2 R_{\odot}$ ) in figure 12. The initial configuration is  $a = 4 R_{\odot}$ ,  $e = 0.2$ ,  $i = 0$ , and we again consider the two cases of a high-spinning star ( $0.9 \omega_{\text{break}}$ ) and a low-spinning star ( $10^{-5} \omega_{\text{break}}$ ).

In the high-spinning case, magnetic braking pushes  $\omega_{\star}$  below corotation, and Hut's stability condition is recovered within a short timescale. Below corotation, tides are too inefficient for synchronizing the spin within the main-sequence lifetime. The same result was found by BO2009 (see their figure 3). The difference is

that we use a different calibration factor causing tides in our model to be weaker. This is shown expressing the tidal calibration factor  $K/T$  as  $\frac{3}{2Q'} \frac{1}{\omega_{\text{orb}}} \frac{GM_{\star}}{R_{\star}^3}$ . This leads to  $K/T \approx 7 \times 10^{-9}$  for the chosen initial conditions and  $Q' = 10^6$ , whereas in our model  $K/T \approx 10^{-11}$ , for every value of the initial spin. The weaker tides cause magnetic braking to spin down the star even more significantly below corotation.

In the BH-LMXB case, a condition in which  $\dot{\omega}_{\star, \text{MB}} = \dot{\omega}_{\star, \text{tid}}$  is reached. This does not happen in the planetary case. The planetary system typically goes through one or two main evolutionary phases, each driven either by magnetic braking or by the tidal torque. In the high spin case, the first phase is driven by MB until the spin finds its-self below corotation, at which point the evolution is driven by the tidal interaction. In the low-spin case, the whole evolution is driven by tides. This overall behaviour of the solution persists in case the calibration factor is the one in BO2009. The stellar spin does not converge to the quasi-equilibrium characterized by  $\omega_{\star} = \omega_{\text{eq}}$ . In both tidal models,  $\omega_{\text{eq}}$  is much smaller than typical  $\omega_{\text{eq}}$  in BH-LMXBs (the corresponding  $P_{\star, \text{eq}}$  is  $\approx 21$  days -see dotted line in the left panel of figure 12- and  $\approx 3$  days in BO2009 model for tides). We will further comments on the absence or presence of the quasi-equilibrium state in section 6.1. The only difference between the evolution in our model and in BO2009 one, is that in the low-spinning case, the time it takes for tides to significantly spin-up the star is shorter.

In the high-spin case, once  $\omega_{\star}$  has been brought by MB below corotation (at  $t \approx 10^{-3} t_{\text{MS}}$ ), tides start removing angular momentum from the orbit, the binary shrinks, and the solution approaches the low-spinning solution, since the star now spins too slowly for magnetic braking to be effective.

In both cases of a high-spinning star and a low-spinning star, tides more easily bring changes to the orbit than to the star, due to the high ratio  $J_{\star}/J_{\text{orb}}$  (see figure 3), and in neither case the RLO-configuration is synchronous, due to low mass-ratio, unlike the BH-LMXB case.

In the middle panel of figure 12 we also show the evolution in the non-coupled method, when taking  $\tau_{\text{circ}} = e/\dot{e}$  (thin light-grey lines), and  $\tau_{\text{circ}} = (e/\dot{e})|_{e \approx 0, \omega_{\star} = \omega_{\text{orb}}}$  (thin dark-grey lines). Neglecting the spin of the star results in a different evolution: the circularization timescale is overestimated. At these large values of  $J_{\star}/J_{\text{orb}}$ , it is essential to follow the coupled evolution of the



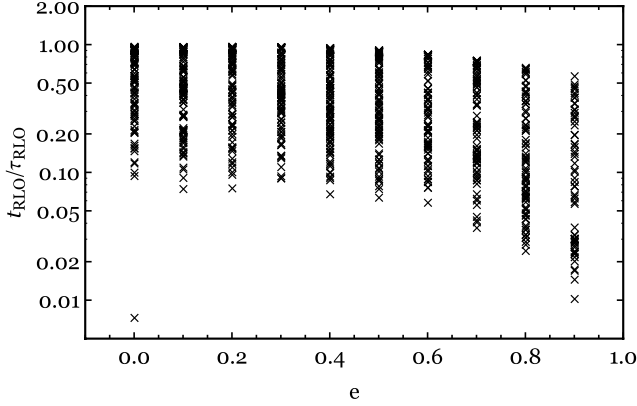


**Figure 9.** Ratio between the time it takes to reach RLO in the coupled and non-coupled method for 1000 black-hole low-mass X-ray binaries undergoing RLO within the MS-lifetime. In the non coupled method, we take  $\tau_{\text{RLO}}$  as  $\tau_{\text{circ}} + t_{\text{VZ}}$  (see text for details).

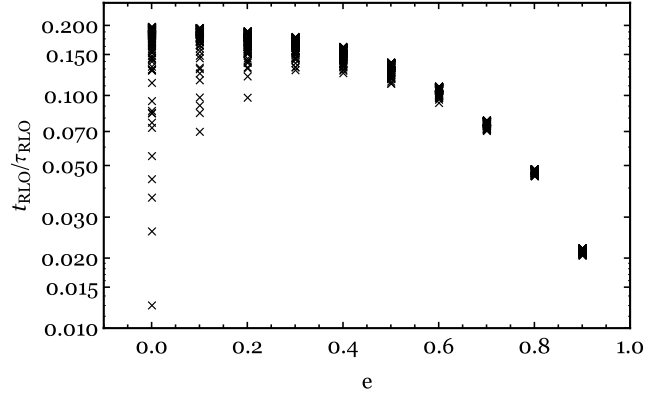


**Figure 10.** Ratio between the time it takes to reach RLO in the coupled and non-coupled method for 1000 black-hole low-mass X-ray binaries undergoing RLO within the MS-lifetime. In the non coupled method, we take  $\tau_{\text{RLO}}$  as  $\tau_{\text{VZ}}$  (see text for details).

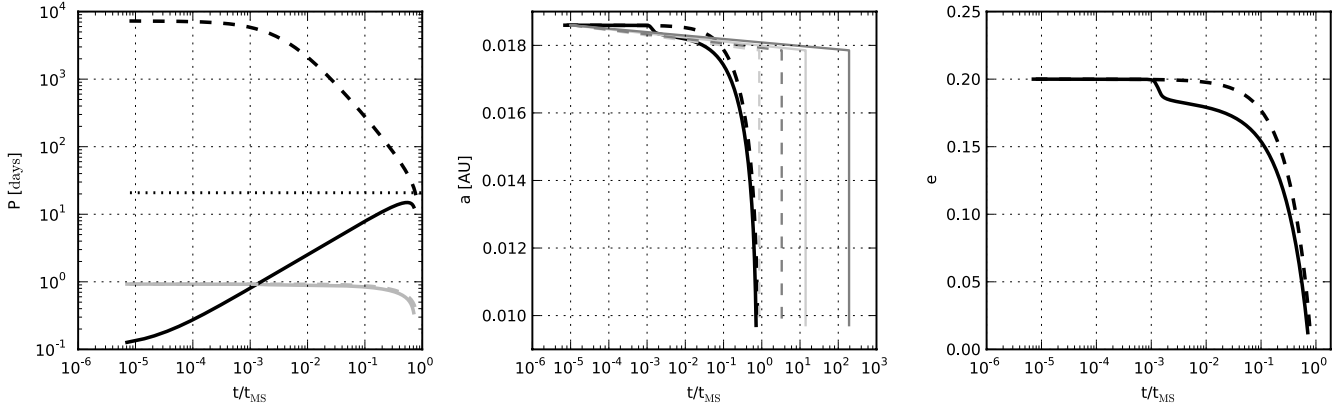


**Figure 12.** Evolution of an eccentric and coplanar planetary system under the effect of tides and magnetic braking. The system contains a Hot-Jupiter and a sun-like star. Initial orbital parameters are  $a = 4 R_{\odot}$ ,  $e = 0.2$ ,  $i = 0$ . We consider both a high-spinning star ( $\omega_{\star} = 0.9 \omega_{\text{break}}$ ) and a low-spinning star ( $\omega_{\star} = 10^{-5} \omega_{\text{break}}$ ). In all panels, solid lines correspond to high-spin, dashed lines to low-spin. In the left panel, the grey lines represent the evolution of the orbital period, the black lines of the stellar period. The dotted line in the same panel represents the value of  $\omega_{\text{eq}}$  (see text for details). In the center panel, the two thick lines represent the evolution of the orbital separation in our integration. In the same panel, the thin dark-gray lines represent the evolution of the orbital separation in the non-coupled method when taking  $\tau_{\text{circ}} = (e/\dot{e})|_{e \approx 0, \omega_{\star} = \omega_{\text{orb}}}$ ; light-gray lines when taking  $\tau_{\text{circ}} = e/\dot{e}$ . The right panel shows the evolution of the eccentricity.

orbital and rotational elements.

#### 4.2.2 An illustrative example of the evolution in the misaligned case

Due to the high ratio  $J_{\star}/J_{\text{orb}}$ , we expect tides to be inefficient in washing away any initial misalignment. In figure 13, we show the evolution of the planetary system for an initial configuration  $a = 3 R_{\odot}$ ,  $e = 0$ ,  $i = 160^{\circ}$ . The rate of alignment is larger in the low-spin case, whereas in the high-spin case, the star rotational angular momentum is too large for being affected by the tidal torque, and the system reaches RLO while being in a non-coplanar configuration. We might wonder what would happen to a retrograde orbit in the absence of magnetic braking. Taking the semi-major axis decay rate for a misaligned orbit (equation 2) and considering a circular case, the  $i$ -dependence of  $\dot{a}$  can be written as:

$$\frac{da}{dt} \propto - \left( 1 + \frac{\omega_{\star} |\cos i|}{\omega_{\text{orb}}} \right) \quad (18)$$

The orbit would undergo an initial decay, with a larger rate for larger inclinations. This is an interesting way of shrinking the orbital separation, though the initial orbital separation has to be already comparable to  $a_{\text{RLO}}$  for RLO to happen on the MS. For example, for the case of an initial misalignment of  $160^{\circ}$ , the maximum initial orbital separation is  $\approx 1.5 a_{\text{RLO}}$ . The same orbital decay due to  $\omega_{\star} \cos i < \omega_{\text{orb}}$  happens in a BH-LMXB. In this case however, the system always reaches alignment and synchronization within the MS-lifetime for sufficiently tight initial orbits, since the tidal torque is much larger.

#### 4.2.3 Population study

We do a population study for the planetary system too, drawing the initial conditions in the same way as we did for the BH-LMXB case (see figures 14 and 15). In the non-coupled method,  $\tau_{\text{circ}}$  is again  $e/\dot{e}$ .

Again we see that  $a_{\text{circ}}$  typically overestimates the actual orbital separation at  $e = 0$ . Concerning the ratio of the timescales, it

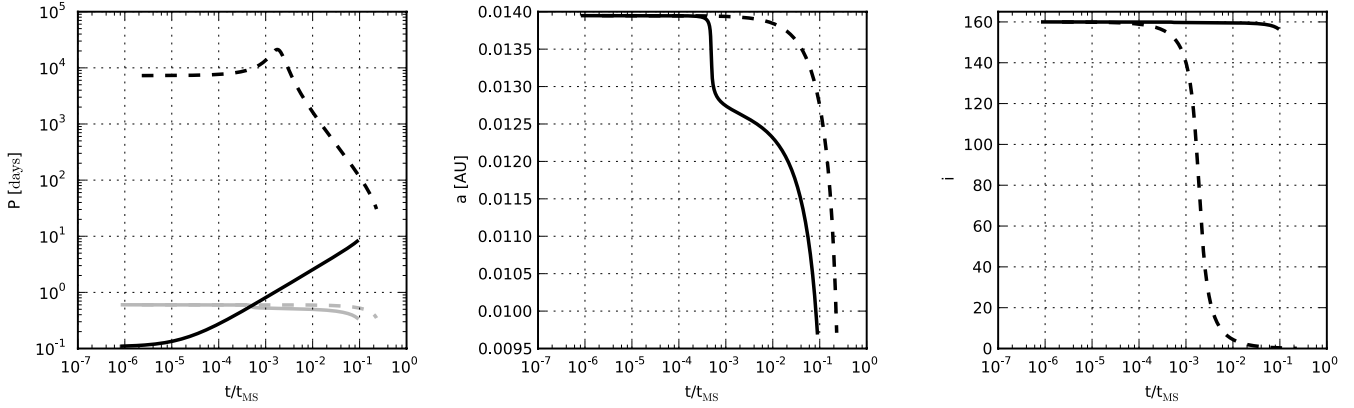


**Figure 13.** Evolution of an eccentric and misaligned planetary system under the effect of tides and magnetic braking. The system consists of a Hot-Jupiter and a sun-like star. Initial orbital parameters are  $a = 3 R_{\odot}$ ,  $e = 0$ ,  $i = 160^{\circ}$ . We consider both a high-spinning star ( $\omega_{\star} = 0.9 \omega_{\text{break}}$ ) and a low-spinning star ( $\omega_{\star} = 10^{-5} \omega_{\text{break}}$ ). In all panels, solid lines correspond to high-spin, dashed lines to low-spin. In the left panel, the grey lines represent the evolution of the orbital period, the black lines of the stellar period. In the center panel, we show the evolution of the orbital separation. The right panel shows the evolution of the misalignment angle.

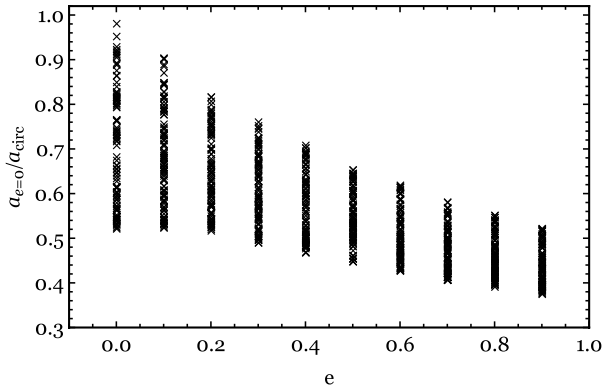


**Figure 14.** Ratio between the orbital separation at  $e = 0$  and  $a_{\text{circ}}$  for 1000 planetary systems undergoing RLO within the MS-lifetime.

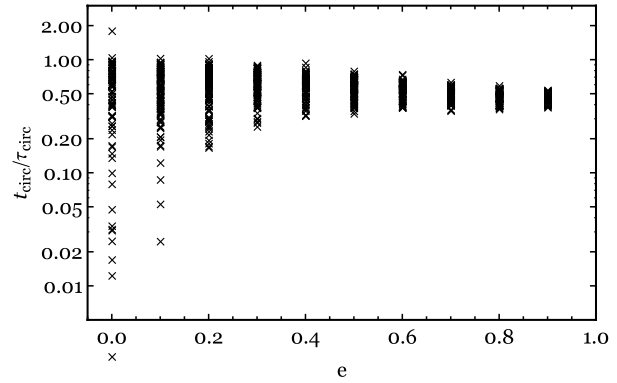


**Figure 15.** Ratio between the time it takes to reach circularization in the coupled and non-coupled method for 1000 planetary systems undergoing RLO within the MS-lifetime.

spans a range of  $\approx [10^{-2}-1]$ . This is consistent with the example of figure 12.

## 5 Wind Braking

While most low-mass stars are magnetic, due to the dynamo processes undergoing in their convective envelopes, only a fraction of intermediate/high-mass stars show magnetic fields. This fraction is smaller than about 15% of the total population, see [Donati & Landstreet 2009](#). When the massive star is magnetic, the stellar wind becomes an analogue of the magnetic-wind in a low-mass star, the only difference being that mass loss is non-negligible anymore. We will take into account the effect of the mass-loss on the binary evolution adding a mass-loss term both in the orbital separation rate and in the spin-frequency rate. We will show that neglecting the spin-down rate due to the mass-loss leads to a different evolution.

### 5.1 Tides coupled with wind braking

Mass loss in a stellar wind removes angular momentum from a rotating star. We assume that the wind is radial and isotropic; the wind can hence be modeled as a spherical shell decoupling from the star

at a certain *decoupling radius*  $r_d$ . If the star is non magnetic,  $r_d$  is the radius of the star  $R_{\star}$ ; whereas if it is magnetic,  $r_d$  is the magnetospheric radius  $r_M$ , i.e. the radius out to which the material corotates with the star.

Expressing the decoupling radius in terms of the stellar radius as  $r_d = \gamma R_{\star}$ , the rate of angular momentum lost is then:

$$\frac{d\vec{J}_{\star}}{dt} = \frac{2}{3} \dot{M}_{\star} \omega_{\star} \gamma^2 R_{\star}^2 \vec{e}_{\omega} \quad (19)$$

where  $\omega_{\star}$  is the rotational frequency of the star. This expression coincides with the the well-known prescription for the angular-momentum loss in a stellar wind by [Weber & Davis 1967](#), when parametrizing the Alfvén radius in terms of the stellar radius. It is valid both for a stellar wind decoupling at the stellar surface ( $r_d = R_{\star}$ ), and for a wind which is forced to corotate out to  $r_d$  by a purely radial magnetic field. For a different field geometry this expression becomes:

$$\frac{d\vec{J}_{\star}}{dt} = \frac{2}{3} \dot{M}_{\star} \omega_{\star} R_{\star}^2 \gamma^n \vec{e}_{\omega} \quad (20)$$

recovering the purely-radial field configuration for  $n = 2$  ([Kawaler 1988](#)).

We assume that the wind decouples from the binary at  $r_d$ ,

without further interaction with the binary components. This is the so-called *fast-wind* approximation, motivated by the fact that typical wind speeds are larger than typical orbital speeds. In a neutron-star high-mass X-ray binary containing a NS of  $1.4 M_\odot$  and a  $15 M_\odot$  star,  $v_{\text{orb}} < 600$  km/s for  $a > a_{\text{RLO}}$ . Taking as wind-velocity  $v_{\text{wind}}$  the escape-velocity from the star, we obtain  $v_{\text{wind}} \approx 1000$  km/s.

To obtain the spin-down rate, we use the mass-radius relation for a ZAMS star, and we assume that the radius of gyration does not change during the evolution on the MS:

$$\frac{d\omega_\star}{dt} = -\frac{\omega_\star}{M_\star} \dot{M}_\star - \frac{2\omega_\star}{R_\star} \frac{dR_\star}{dM_\star} \dot{M}_\star + \frac{2}{3} \frac{\dot{M}_\star r_d^2 \omega_\star}{k^2 M_\star R_\star^2} \quad (21)$$

If the star is in a binary, the wind won't take away rotational angular momentum only, but orbital angular momentum as well. This effect adds up to the tidal effect on the orbital separation as a non-negative term  $-a\dot{M}_\star/M$  in the orbital separation rate.

The full evolutionary equations for an eccentric and misaligned binary system under the coupled effect of tides and a massive stellar wind are equations 2, 3, 4, 5, to which we add the term in equation 21 and the term:

$$\frac{da}{dt} = -\frac{\dot{M}_\star}{M} a \quad (22)$$

and we use the calibration factor  $(K/T)_r$  for a radiative envelope.

The mass-loss for a sun-like star on the MS is negligible, thus we can neglect the term in eq. 22. The mass-loss effect on the spin-down rate is reduced to the third term in equation 21. Even if the mass-loss is small, this term can be significant, when the decoupling radius is large ( $r_d \approx 20 R_\odot$  for the Sun). The magnetic-braking law 1 is empirical, and it can be recovered through MHD-theory coupled with theoretical studies of the dynamo process. [Kawaler 1988](#) studied the angular momentum loss in low-mass stars and showed that Skumanich's law is recovered taking  $n = 3/2$  in equation 20 and neglecting the change in mass and radius of the star.

The mass-loss in a fast isotropic wind always widens the orbit of a binary formed by point-like components, due to the decrease in binding energy. However, if the mass-losing star suffers from tidal deformation, the tides-induced torque can prevent the widening thanks to the redistribution of angular momentum. When  $\omega_\star < \omega_{\text{eq,tid}}$ , where

$$\omega_{\text{eq,tid}} = f_2(e^2) \omega_{\text{orb}} \left[ \frac{1}{f_5(e^2)(1-e^2)^{3/2}} \right], \quad (23)$$

the tidal torque term in the spin rate is positive (see equation 4). This means that tides bring angular momentum from the orbit to the star, counteracting the effect of the mass loss. We note that  $\omega_{\text{eq,tid}}$  is alternatively referred to as *pseudo-synchronization* frequency, the synchronization frequency on an eccentric orbit (see [Hut 1981](#)). This is an *instantaneous-equilibrium* spin frequency, since orbital properties are still evolving. When the orbit is circular, this pseudo-synchronization frequency coincides with the orbital frequency.

In the next paragraph, we will estimate for which value of  $\gamma$  the effect of the tidal torque in decreasing the orbital separation is stronger than the effect of the orbital angular momentum loss in increasing it.

A few of the previous works on the evolution of HMXBs have integrated the tidal equations coupled with the angular momentum loss in the wind (see for example [Wong et al. 2012](#)). What we do differently, is to include in our set of equations the misalignment

between the spin of the orbit and the stellar spin, and to parametrize the angular momentum loss in the wind in terms of  $\gamma$ , following the orbital evolution in a semi-analytical way and highlighting some interesting outcomes of the coupling between tides and a massive stellar wind.

## 5.2 Results

### 5.2.1 Timescale considerations

Let's assume we have a synchronized, circular and coplanar orbit. The orbital separation changes due to the loss of orbital angular momentum (term of equation 22). It also changes due the tidal redistribution of angular momentum. The star loses rotational angular momentum in the wind, and the tidal torque counteracts this effect. The effect of the tidal torque on the orbital separation can then be found from  $\dot{J}_{\text{orb}} = \dot{J}_\star$ , which gives the orbital separation decay rate:

$$\left. \frac{da}{dt} \right|_{\text{tid}} = -\frac{4}{3} \frac{|\dot{M}_\star| \gamma^2 R_\star^2 M}{M_{\text{comp}} M_\star a} \quad (24)$$

Taking the ratio between  $\dot{a}|_{\text{ML}}$  and  $\dot{a}|_{\text{tid}}$ , we get:

$$\left. \frac{da}{dt} \right|_{\text{tid}} = \frac{4}{3} \left( \frac{\gamma R_\star}{a_2} \right)^2 q \left. \frac{da}{dt} \right|_{\text{ML}} \quad (25)$$

where  $a_2$  is the distance of the star from the binary centre-of-mass,  $a_2 = (M_{\text{comp}}/M)a$ . The effect of the loss of  $J_{\text{orb}}$  is larger when the star is further away from the centre-of-mass (i.e. the larger  $a_2$  is). Whereas the effect of the tidal torque is larger the larger the decoupling radius is (due to  $J_\star$ -loss being larger), and/or the larger is the mass-ratio (due to the tidal torque dependence on  $q$ ).

We define  $\gamma_{\text{min}}$  as  $\gamma$  such that the condition  $\left. \frac{da}{dt} \right|_{\text{tid}} = \left. \frac{da}{dt} \right|_{\text{ML}}$  is met. The tidal torque is more effective than the orbital angular momentum loss in changing the orbital separation for  $\gamma > \gamma_{\text{min}}$ :

$$\gamma_{\text{min}}(q, \eta) = \sqrt{\frac{3}{4q}} \frac{q}{1+q} \frac{\eta}{f(1/q)} \quad (26)$$

where we parametrized the orbital separation in terms of the RLO-separation,  $a = \eta a_{\text{RLO}}$ .

For a NS-HMXB composed of a  $1.4 M_\odot$  NS and a  $15 M_\odot$  companion §, the mass ratio is  $q \approx 0.09$ , and taking  $\eta = 2$ , we find  $\gamma_{\text{min}} \approx 0.83$ . For the illustrative integration showed in figure 18,  $\eta = 1.5$ , and the corresponding  $\gamma_{\text{min}}$  is  $\approx 0.6$ . This means that *wind-braking* ¶ wins over the mass-loss effect for every value of gamma. This remains valid when the companion mass spans a range of  $[10 - 50] M_\odot$  in mass.

For a BH-HMXB composed of a  $8 M_\odot$  BH and a  $15 M_\odot$  companion,  $q \approx 0.53$ . We calculate  $\gamma_{\text{min}}(q, 2) \approx 1.9$  and  $\gamma_{\text{min}}(q, 1.5) \approx 1.6$ . The latter  $\gamma_{\text{min}}$  corresponds to the initial conditions of figure 19. For smaller  $\gamma$ , we expect the orbital separation to grow in time (see dotted line in figure 19). As another example we calculate the minimum gamma for the BH-HMXB Cygnus X-1. Its component masses are  $M_\star \approx 19 M_\odot$  and  $M_{\text{comp}} \approx 15 M_\odot$  ([Orosz et al. 2011](#)). The correspondent  $\gamma_{\text{min}}$  for  $\eta = 2$  is  $\approx 2$ .

In case wind braking is effective in shrinking the orbit, we

§ There are at least 3 known NS-HMXBs with similar component masses, see [van Kerkwijk et al. 1995](#), [van der Meer et al. 2005](#), [Val Baker et al. 2005](#).

¶ We name "wind braking" (WB) the shrinking of the semi-major axis due to the tidal counteracting effect on the loss of rotational angular momentum, in analogy with magnetic braking.

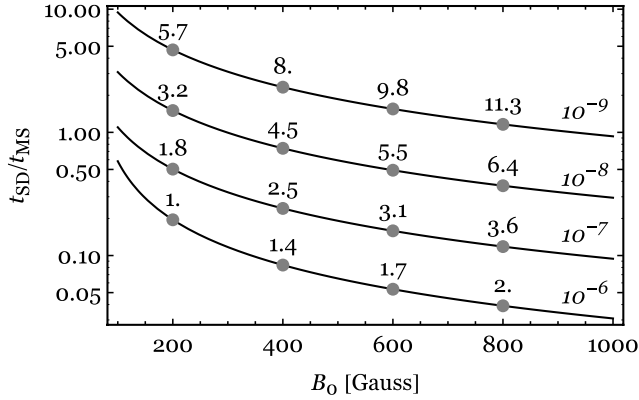


**Figure 16.** Ratio between the spin-down timescale and the MS-lifetime for a star of mass  $15 M_{\odot}$ , as a function of the stellar surface magnetic field for different mass losses,  $|\dot{M}_{\star}| = \{10^{-9}, 10^{-8}, 10^{-7}, 10^{-6}\} M_{\odot} / \text{yr}$ . Values of  $\gamma$  as a function of  $B_0$  and  $\dot{M}_{\star}$  are indicated along the curves.

wonder for which values of mass-loss in the wind and of  $\gamma$ , the binary is shrunk down to RLO within the MS-lifetime. The spin-down timescale due to the angular momentum loss in the wind is:

$$\frac{1}{\tau_{\text{SD}}} = \frac{|\dot{\omega}_{\star}|_{\text{SD}}}{\omega_{\star}} \quad (27)$$

where  $\dot{\omega}_{\star}|_{\text{SD}}$  is as in equation 21. The spin-down timescale is then a function of the mass-loss and of the decoupling radius. If the star is magnetic, we use the fact that the decoupling radius can be defined as the distance from the star at which the ram pressure of the flow and the magnetic pressure are balancing each other. Justham et al. 2006 show that:

$$r_d \sim B_0^{1/2} R_{\star}^{13/8} |\dot{M}_{\star}|^{-1/4} (GM_{\star})^{-1/8} \quad (28)$$

where  $B_0$  is the surface stellar magnetic field. We use this expression for  $r_d$  in order to rewrite the spin-down timescale 27 in terms of  $B_0$  and of  $\dot{M}_{\star}$ . We are interested in those combinations of  $\dot{M}_{\star}$  and  $B_0$  for which the star is sufficiently spun-down on the MS.

In figure 16 we show the ratio between the spin-down timescale and the MS-lifetime for a star of mass  $15 M_{\odot}$  ( $\tau_{\text{MS}} \approx 1.15 \times 10^7$  years) as a function of the stellar surface magnetic field. Different curves are presented for different wind mass-losses. Mass-losses are chosen as  $|\dot{M}_{\star}| = \{10^{-9}, 10^{-8}, 10^{-7}, 10^{-6}\} M_{\odot} / \text{yr}$ . For larger  $B_0$ , the ratio decreases, since a stronger field guarantees the corotation of the field lines out to large distances from the star, where the rotational angular momentum carried away by the wind is larger. For the same magnetic field, the spin-down timescale is smaller for larger mass-loss, since a higher mass-loss brings away a larger angular momentum. Along the curves we also indicate the value of  $\gamma = r_d/R_{\star}$  for that combination of  $B_0$  and  $\dot{M}_{\star}$ . For the same field strength at the surface  $B_0$ , the decoupling radius is larger for a smaller mass loss. This is due to the fact, that for a smaller ram pressure (smaller  $\dot{M}_{\star}$ ), the balancing magnetic pressure ( $\sim B_0^2/r_d^2$ ) is smaller; if the surface B-field is fixed, the decoupling radius has therefore to be larger.

Typical magnetic fields of the subset of magnetic O-B stars and of Ap-Bp stars are of the order of hundreds to thousands Gauss (Donati & Landstreet 2009). We compute their typical main-sequence wind mass-loss using the fitting formula by Nieuwenhuijzen & de Jager 1990, who parametrize the wind-mass loss in terms of the luminosity, the mass and the radius of the star. Evolving a

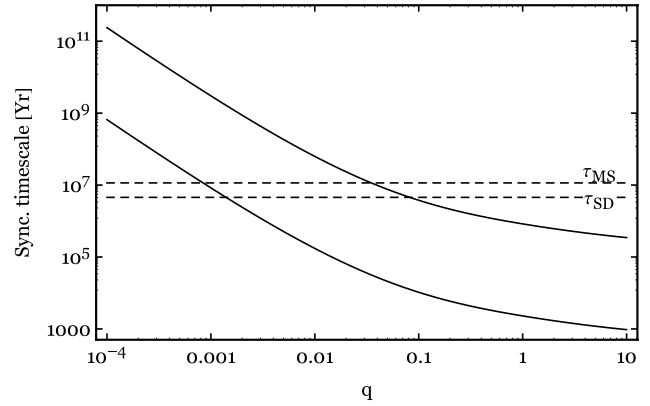


**Figure 17.** Synchronization timescales for a binary composed of a  $15 M_{\odot}$  star as a function of the binary mass-ratio  $q$ , both for an orbital separation  $a = a_{\text{RLO}}$  and  $a = 2 a_{\text{RLO}}$ . The horizontal dashed lines show the spin-down timescale and the MS-lifetime. The spin-down timescale has been computed for  $\gamma = 2$  and  $\dot{M}_{\star} = -10^{-7} M_{\odot} / \text{yr}$ .

star with a ZAMS mass of  $15 M_{\odot}$ , with the SSE code by Hurley et al. 2000 embedded in the Astrophysics Multipurpose Software Environment AMUSE (Portegies Zwart et al. 2009), we extract the luminosity and radius of the star. We find a wind mass-loss in the range  $10^{-8} - 10^{-7} M_{\odot} / \text{yr}$  on the MS.

As an example, for a decoupling radius  $\gamma = 2$  and a mass-loss  $|\dot{M}_{\star}| = 10^{-7} M_{\odot} / \text{yr}$ , we obtain an estimate for the required stellar magnetic field of  $\sim 250$  Gauss. For these values of  $B$  and  $\dot{M}_{\star}$ , we expect the binary to shrink down to RLO.

In figure 17 we show the synchronization timescales calculated using eq. 15 for a binary formed by a star of mass  $15 M_{\odot}$  as a function of the mass-ratio  $q$ , both for an orbital separation  $a = a_{\text{RLO}}$  and  $a = 2 a_{\text{RLO}}$ . The assumptions we make on the decoupling radius and the mass-loss rate are  $\gamma = 2$  and  $\dot{M}_{\star} = -10^{-7} M_{\odot} / \text{yr}$  which, as can be seen in figure 16, allow for a short spin-down timescale ( $\tau_{\text{SD}}/\tau_{\text{MS}} \approx 0.3$ ). For our cases of interest of a NS-HMXB ( $q \approx 0.1$ ) and of a BH-HMXB ( $q \approx 0.5$ ),  $\tau_{\text{sync}}$  is short, hence we expect the binaries to rapidly reach the synchronous state.

### 5.2.2 Wind braking in NS-HMXBs and BH-HMXBs

We integrate the coupled equations of section 5.1 for a binary composed of a neutron star of mass  $1.4 M_{\odot}$  and a  $15 M_{\odot}$  star, with an orbital separation  $a = 14 R_{\odot}$  and eccentricity  $e = 0.2$ .

We take different combination for the mass-loss rate and the decoupling radius:  $\{|\dot{m}|, \gamma\} = \{\{10^{-7}, 2\}, \{10^{-8}, 2\}, \{10^{-7}, 1\}\}$  (where  $\dot{m}$  is the mass-loss rate in solar masses per year). For each of these three combinations, we also calculate the evolution when neglecting the mass-loss terms in the spin-frequency rate (terms in eq. 21), which we call *standard* model. Concerning the spin frequency, we take a star rotating at 20% of its break-up frequency, which is a typical lower-limit on the natal rotating speed of a high-mass star (see Donati & Landstreet 2009). The associated ratio  $\omega_{\star}/\omega_{\text{eq, tid}}$  is  $\approx 0.7$ . We must point out that this is valid in the assumption that the binary evolution prior and during the compact object formation does not affect the stellar spin. Anyhow, what is important for our study, is to compare the initial  $\omega_{\star}$  with  $\omega_{\text{eq, tid}}$  of equation 23.



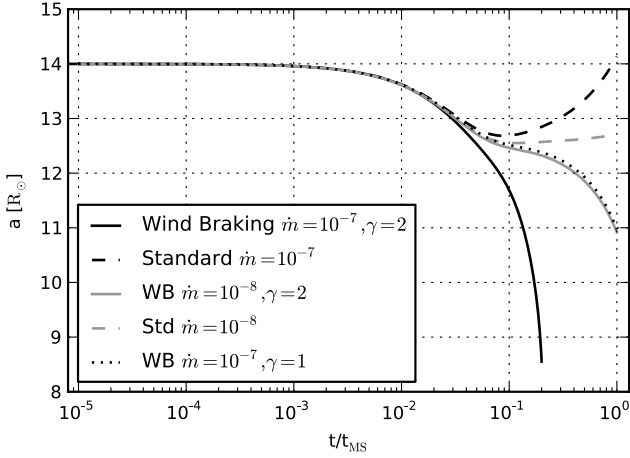


**Figure 18.** Evolution of a NS-HMXB under the effect of tides and a massive stellar wind (solid lines). Masses of the components are  $M_* = 15 M_\odot$  and  $M_{\text{comp}} = 1.4 M_\odot$ . Initial orbital parameters are  $a = 14 R_\odot$ ,  $e = 0.2$ ,  $\omega_* = 0.2 \omega_{\text{break}}$ . We also show the evolution in the standard scenario, when the mass-loss has an effect on the orbital separation only (dashed lines).

Initial conditions with  $\omega_* > \omega_{\text{eq,tid}}$  are of no interest, since the binary widens, preventing RLO.

We show in figure 18 the outcome of the evolution. The first phase of the evolution is driven by tides, until synchronization is achieved (at  $t \approx 6 \times 10^{-2} t_{\text{MS}}$ ). At this moment, the different prescriptions on the decoupling radius and on the mass-loss rate start playing a role. When dealing with WB, the evolution is faster for a larger mass-loss. If the mass-loss is too small, the binary does not reach RLO within the MS-lifetime. If the wind-braking spin-down is not taken into account, the orbital separation increases once the synchronous state is achieved, as expected due to the positive wind-mass loss term in the orbital separation rate. For the wind-braking solutions, once synchronization is achieved, the tidal torque replenishes the rotational angular momentum reservoir of the star, counteracting the spin-down effect of the wind, and removing angular momentum from the orbit: this is exactly what happens in the magnetic braking case.

We also note how the two solutions with  $\{\dot{m}, \gamma\} = \{10^{-7}, 1\}$  and  $\{\dot{m}, \gamma\} = \{10^{-8}, 2\}$  only slightly differ from each other. This is due to the degeneracy in  $\dot{m}$  and  $\gamma$ . The spin-down timescale is  $\tau_{\text{SD}} \approx 2\tau_{\text{MS}}$  and  $\tau_{\text{SD}} \approx 4\tau_{\text{MS}}$  for the two choices respectively.

Solving the coupled equations for different values of the initial stellar spin, we note that if the initial spin is too low, tides won't manage to synchronize the star on the evolutionary timescale. What happens is that the orbit keeps shrinking due to the tidal torque only, and there is no appreciable difference between the tides-only solution and the WB-solution. The initial binary configuration ( $a, e, \omega_*$ ) which gives rise to an evolution of the wind-braking type, satisfies three properties. The stellar spin is less than  $\omega_{\text{eq,tid}}$ . The configuration allows for tides to synchronize the spin within the MS-lifetime. Lastly, it allows the wind to significantly remove angular momentum from the orbit bringing the system to RLO within the MS-lifetime.

We follow the evolution under tides and a massive stellar wind for a BH-HMXB as well. We take as initial orbital parameters  $a = 17 R_\odot$ ,  $e = 0.2$ , and a star rotating at  $0.2 \omega_{\text{break}}$ . We show in

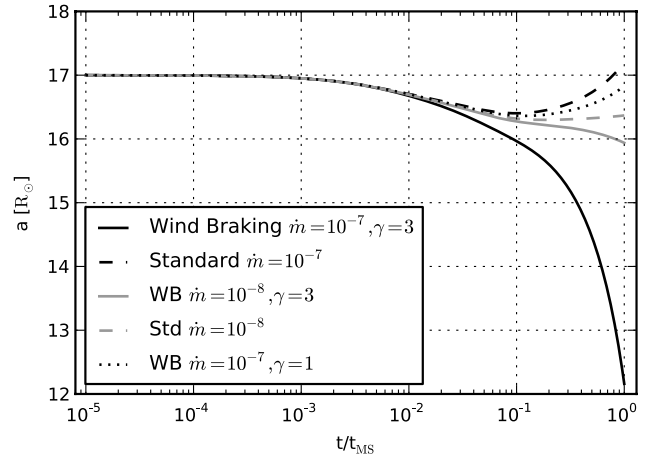


**Figure 19.** Evolution of a BH-HMXB under the effect of tides and a massive stellar wind (solid lines). Masses of the components are  $M_* = 15 M_\odot$  and  $M_{\text{comp}} = 8 M_\odot$ . Initial orbital parameters are  $a = 17 R_\odot$ ,  $e = 0.2$ ,  $\omega_* = 0.2 \omega_{\text{break}}$ . We also show the evolution in the standard scenario, when the mass-loss has an effect on the orbital separation only (dashed lines).

figure 19 the result of the integration. We note how the solution with  $\{\dot{m}, \gamma\} = \{10^{-7}, 1\}$  (dotted line) differs from the solution corresponding to the same pair  $\{\dot{m}, \gamma\}$  for a NH-HMXB. This is due to the fact that  $\gamma R_*/a_2$  is smaller for a BH-HMXB since  $a_2$  is larger; this means that the tidal effect on the orbital separation is smaller. This was expected, since  $\gamma = 1$  is less than the minimum value for having wind-braking type solutions in a BH-HMXB of this type.

## 6 Discussion

In this section, we would like to comment on the calibration of magnetic braking and of tides that we chose. We also comment briefly on how our results on the evolution of a planetary system might change when considering the tides raised by the star on the planet as well.

(i) The empirical Skumanich law was derived measuring the equatorial velocity of G-type MS-stars with rotational velocities between 1 – 30 km/s. It is therefore arguable whether it is still applicable to fast rotators, like the ones in compact binaries where the star, being synchronized with the orbit, rotates at velocities of hundreds km/s. For this reason, *saturated* magnetic-braking laws have been suggested, in which the spin-down rate saturates once the star-frequency reaches a critical value (see Knigge et al. 2011, for reviewing the different MB-prescriptions). We adopt Ivanova & Taam 2003 prescription for MB in the formulation chosen by Ivanova & Kalogera 2006:

$$\dot{J}_{*,\text{MB}} = -K_j \left( \frac{R_*}{R_\odot} \right)^4 \begin{cases} (\omega_*/\omega_\odot)^3 & \text{for } \omega \leq \omega_x \\ \omega_*^{1.3} \omega_x^{1.7} / \omega_\odot^3 & \text{for } \omega > \omega_x \end{cases} \quad (29)$$

where  $\omega_\odot \approx 3 \times 10^{-6} \text{ s}^{-1}$  is the angular velocity of the Sun,  $K_j = 6 \times 10^{30} \text{ dyn cm}$ , and the critical angular velocity is  $\omega_x = 10 \omega_\odot$ . From this law, the spin-down rate  $\dot{\omega}_*$  is derived.

We integrate the tidal equations coupled with the previous MB-prescription for the BH-LMXB shown in figure 5, taking a star

spinning at  $0.9 \omega_{\text{break}}$ , a value which is much larger than the critical angular frequency  $\omega_x$ , thus the spin-down rate scales as  $\omega_*^{1.3}$ . In this prescription magnetic braking is much less efficient than in the [Verbunt & Zwaan 1981](#) prescription, hence the binary does not reach RLO within the MS-lifetime ( $a \approx 5 a_{\text{RLO}}$  at  $t = t_{\text{MS}}$ ). In the first phase of the evolution, MB spins down the star while tides lead to a slight widening of the orbit, unlike what happens in our formulation. In this case too  $\omega_*$  converges to  $\omega_{\text{eq}}$ , which corresponds to the value at which  $\dot{\omega}_{*,\text{MB}} = \dot{\omega}_{*,\text{tid}}$ . After that, the binary shrinks thanks to the coupling tides-MB, however much less significantly than when using [Verbunt & Zwaan 1981](#) prescription for MB.

(ii) There is a factor  $\approx 10^5$  between the timescales in our model and the timescales computed according to BO2009 tidal model. This is due to the fact that  $K/T$  is a function of both  $\omega_*$  and  $\omega_{\text{orb}}$ , through the tidal pumping timescale, whereas the calibration factor in BO2009, is a function of  $\omega_{\text{orb}}$  only. When  $\omega_*$  and  $\omega_{\text{orb}}$  differs strongly (like in the case when  $\omega_* = 0.9 \omega_{\text{break}}$ ) our tidal calibration factor is significantly reduced. Instead, when  $\omega_* \approx \omega_{\text{orb}}$ , the ratio between the two tidal calibration factors is 1 – 2 for every mass ratio, leading to similar timescales.

(iii) We wonder whether our results are a function of the tidal calibration we choose. In the BH-LMXB case, a different tidal calibration factor will affect the time it takes for reaching the circular and synchronized configuration. However, since this timescale is very short compared to the MS-lifetime, independently of the chosen calibration, we expect no appreciable difference when taking a different tidal calibration factor. Once synchronization is achieved, the evolution of the system is well described by equation 13, that is, the calibration of tides does not play a role anymore. Integrating the tidal equations according to BO2009 model for tides and coupling them with magnetic braking, we note that when the star is initially high-spinning, the orbital separation increases initially, that is in the first phase of the evolution tides and MB are both at work; this will lead to a larger circularized orbital separation, but the final outcome of the evolution of a BH-LMXB is not significantly affected. As a more quantitative test, we use the maximal initial orbital separation  $a_{\text{max}}$  such that the BH-LMXB reaches RLO within the MS-lifetime; the ratio between  $a_{\text{max}}$  in our model and  $a_{\text{max}}$  in BO2009 model of tides, is  $\approx 1$ , for all values of the initial eccentricity.

In the planetary system case, the situation is different. A high-spinning star is typically spun-down below corotation. At this point, MB has a negligible effect, unlike the tidal interaction, and, if the initial configuration is close enough, tides bring the system towards RLO. The stronger tides are, the faster the evolution towards RLO. Looking at the maximal initial orbital separation so that the planetary system reaches RLO within the MS-lifetime, the ratio between  $a_{\text{max}}$  in our model and  $a_{\text{max}}$  in BO2009 model of tides, is  $\approx 0.3 - 0.4$ .

(iv) When applying our model to the planetary case, we only considered the tide raised by the planet on the star, and not the tide raised by the star on the planet. Since the angular momentum stored in the planet is much less than the orbital angular momentum, due to the compactness of the planet, we expect the planet to rapidly synchronize with the orbit. If tides in the planet are included, we expect circularization to be reached faster, due to eccentricity damping effect of the tide in the planet (see BO2009 and [Rasio et al. 1996](#)). [Matsumura et al. 2010](#) followed the evolution of a Hot Jupiter in an eccentric and misaligned orbit around its host star, accounting for both the tide in the star and in the planet. The stellar tide largely dominates the evolution of the orbital separation and obliquity. Instead, both the tide in the planet and in the star contribute to the damping of the eccentricity, and depending on the

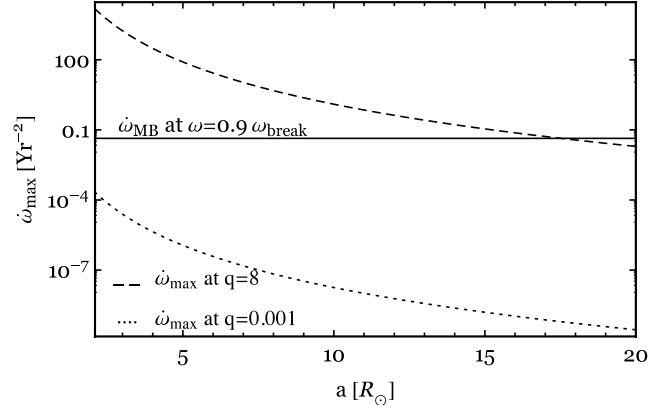


**Figure 20.** Values of  $\dot{\omega}_{\text{max}}$  such that the system can reach the quasi-equilibrium state, as a function of the orbital separation, and calculated for a mass ratio  $q = 8$  and for  $q = 0.001$ . Horizontal lines correspond to the spin-down rate due to MB.

planet tidal quality factor, circularization can be achieved without a significant orbital decay. We expect our main conclusions on the inadequacy of timescale considerations to be preserved, as already predicted by [Jackson et al. 2008](#), who accounted for the tide in the planet.

## 6.1 On the quasi-equilibrium state

The concept of *quasi-equilibrium state* for the spin of the stellar component in a binary, was already introduced by [Dobbs-Dixon et al. 2004](#), for the case of a planetary system containing a star and a Hot Jupiter. At the quasi-equilibrium, the rate of angular momentum loss in the stellar wind is balanced by the rate at which the star gains angular momentum from the orbit as the planet attempts to spin-up the star. The authors give an upper limit for the angular momentum loss in the stellar wind, such that this quasi-equilibrium can be achieved. We use a similar approach, and we calculate the maximum spin-down rate due to MB such that the quasi-equilibrium can be achieved. In order to find  $\omega_{\text{eq}}$ , we put  $\dot{\omega} = 0$  in equation 4, and we take a circular and coplanar orbit. We obtain:

$$\omega_{\text{eq}} = \omega_{\text{orb}} - \frac{1}{3} \frac{1}{K/T} \frac{k^2}{q^2} \left( \frac{a}{R_*} \right)^6 |\dot{\omega}_{\text{MB}}| \quad (30)$$

where  $a$  and  $\omega_{\text{orb}}$  are the orbital separation and the orbital frequency at the quasi-equilibrium state. This quasi-equilibrium spin value is attainable provided that:

$$|\dot{\omega}_{\text{MB}}| < \frac{9}{2Q'} \frac{q^2}{k^2} \frac{GM_* R_*^3}{a^6} = \dot{\omega}_{\text{max}} \quad (31)$$

We note that we have chosen the calibration factor as in BO2009, that is we have replaced  $K/T$  with  $\frac{3}{2Q'} \frac{1}{\omega_{\text{orb}}} \frac{GM_*}{R_*^3}$ , so that the equation  $\dot{\omega} = 0$  could be solvable analytically in terms of  $\omega_{\text{eq}}$ . Condition 31 is typically not fulfilled in a planetary system, whereas it is fulfilled in a BH-LMXB (see figure 20). This is consistent with our results in section 4.

## 6.2 An application to the NS-HMXB Circinus X-1

One way of testing the calibration of tides, is to look at young and detached high-mass X-ray binaries, which still did not have time to circularize. In detached systems, any orbital decay or boost

could be directly associated with the tidal interaction between the two components. Such a study was performed by [Belczynski et al. 2008](#) for LMC X-4, a NS-HMXB. The observed orbital decay of the source,  $P/\dot{P} \approx 10^6$  years, is consistent with an orbital decay driven by the tidal torque when using the calibration factor in equation 10.

Another possible example is Circinus X-1, the youngest known X-ray binary. An upper limit on its age of  $t < 4600$  years has been placed by [Heinz et al. 2013](#), through X-ray studies of its natal supernova remnant. The X-ray emission is thought to be caused by RLO at periastron, hence this binary is semi-detached, unlike LMC X-4. X-ray dip timing shows the binary is undergoing orbital decay ([Parkinson et al. 2003](#) and [Clarkson et al. 2004](#)), with  $P/\dot{P}$  measured to be  $\sim 3000$  yr. The current orbital parameters are  $e \approx 0.45$  and  $P_{\text{orb}} \approx 16.68$  days. [Jonker et al. 2007](#) constrained the radius of the companion star by ensuring the neutron star does not go through the companion at periastron. The surface gravity gives in turn the mass. We use  $M_* = 10 M_{\odot}$  and  $R_* \approx 39 R_{\odot}$  for the mass and radius of the high-mass star, and  $M_{\text{comp}} = 1.4 M_{\odot}$  for the mass of the neutron star. These initial conditions allow us to compute the current timescales for the change in the orbital period  $P/\dot{P} = (2/3)a/\dot{a}$ , using the tidal equations in our model. The only uncertainty is the spin of the companion. When  $\omega_*$  is smaller than  $\omega_{\text{eq,tid}}$ , tidal interaction results in a decay of the orbit. For these initial orbital parameters,  $\omega_{\text{eq,tid}} \approx 1.25 \omega_{\text{break}}$ . The calculated timescales are  $\approx 9 \times 10^3$  years and  $\approx 2 \times 10^4$  years, for  $\omega_*$  varying from 0 and  $0.9 \omega_{\text{break}}$ . One possibility is that tides are more efficient than the ones in our model, by a factor of  $\approx 3$  when taking a non-rotating star. Alternatively, the observed orbital decay is either induced by the mass-transfer itself, or an additional spin-orbit coupling is responsible for it, as suggested by [Heinz et al. 2013](#).

### 6.3 Remarks on our results on the circularization timescale and their consequences

(i) There is a variety of papers in the literature which base their description of the evolution of compact binaries on timescale considerations (see for example, [Kalogera 1999](#), [Yungelson et al. 2006](#), [Pylyser & Savonije 1988](#), [Ma & Li 2009](#)). Since citing all of them does not seem like a sensible choice, we rather show an example of how timescale considerations could fail. [Janssen & van Kerkwijk 2005](#) study a compact binary formed by a pulsar and a low-mass star. The observed eccentricity is  $e \lesssim 0.005$ , while the initial eccentricity is constrained to be  $e \sim 0.7$ . The authors assume an exponential decay of the eccentricity when dealing with the circularization of the binary. We instead integrated our equations to solve for the evolution of the eccentricity of this system. We obtain  $t_{\text{circ}} = 2 \times 10^9$  yr and  $\tau_{\text{circ}} = 6 \times 10^7$  yr for a low-spinning star, and  $t_{\text{circ}} = 4 \times 10^9$  yr and  $\tau_{\text{circ}} = 2 \times 10^{10}$  yr, for a high-spinning star. This result highlights the inadequacy of timescale considerations when studying the evolution of individual systems.

(ii) We would also like to point out that some of the currently used BPS codes might treat tidal interaction using timescale arguments or assuming instantaneous circularization (see for example, [Portegies Zwart & Verbunt 1996](#)). However, our population models for the progenitors of BH-LMXBs show that the population of BH-LMXBs (i.e. the number of systems that start mass transfer on the MS) might not be very different, also given the large uncertainties in the calibration factor.

## 7 Conclusions

(i) The evolution of a binary formed by a point-mass and a star can be solved relatively easily for arbitrary mass-loss, eccentricity, and inclination via coupled differential equations. In this way we can easily investigate how the evolution changes as a function of the binary mass-ratio and of the ratio  $J_*/J_{\text{orb}}$ .

(ii) When tides are coupled with magnetic braking the evolution of a BH-LMXB can be separated into two main phases. The first one is driven either by tides or by magnetic braking, depending on how fast the star is initially rotating. In both cases, the outcome of the first phase of the evolution is that the spin of the star converges to a quasi-equilibrium value at which  $|\dot{\omega}_{*,\text{MB}}| = |\dot{\omega}_{*,\text{tid}}|$ : the effect of the tidal torque and of magnetic braking are balancing each other. From this moment on, every piece of angular momentum lost from the star is subtracted from the orbit.

(iii) In a planetary system instead, tides are too weak, and an initially-high stellar spin is typically brought below corotation. From this point on, the evolution coincides with the evolution in the low-spin case. Unlike the BH-LMXB case, the binary does not reach the quasi-equilibrium state. If the star is initially high-spinning and highly inclined with respect to the orbital angular momentum, the RLO configuration is typically non-coplanar.

(iv) Models which neglect the coupling between tides and winds do not accurately represent the true evolution of compact binaries. The simple estimate  $\tau_{\text{circ}}$  is not a good approximation for the actual change of  $e$  over time, because it does not account for the change in the orbital separation due to changes in the stellar spin. Nor for the fact that  $\dot{e}$  typically increases during the evolution, due to decrease of the semi-major axis, whereas in the estimate  $e/\dot{e}$  the orbital separation  $a$  is assumed to be constant. Furthermore, neglecting the spin leads to an overestimate of the semi-major axis at circularization. It is then essential to consider the coupled evolution of rotational and orbital elements in order to accurately model the evolution of compact binaries. This was already showed previously by [Jackson et al. 2008](#) and [Barker & Ogilvie 2009](#), for the planetary system case.

(v) We have implemented an easy model to follow the evolution of a HMXB under the coupled effect of tides and winds. For particular choices of decoupling radius and mass-loss, wind braking in a high-mass X-ray binary behaves as magnetic braking in a low-mass X-ray binary. The values of decoupling radii and mass-losses which allow for a wind braking-type solution, are consistent with typical magnetic fields and typical mass-losses of high-mass stars.

## 8 Acknowledgments

We thank the anonymous referee whose comments greatly improved the Paper. SR is very grateful to Silvia Toonen for a careful and critical reading, which brought significant improvements to the manuscript. SR is thankful to Adrian Barker for a useful discussion on the calibration of tidal dissipation. The work of SR was supported by the Netherlands Research School for Astronomy (NOVA).

## REFERENCES

- Alexander M. E., 1973, *Ap&SS*, 23, 459
- Barker A. J., Ogilvie G. I., 2009, *MNRAS*, 395, 2268
- Belczynski K., Kalogera V., Rasio F. A., Taam R. E., Zezas A., Bulik T., Maccarone T. J., Ivanova N., 2008, *ApJS*, 174, 223

- Church R. P., Kim C., Levan A. J., Davies M. B., 2012, *MNRAS*, 425, 470
- Clarkson W. I., Charles P. A., Onyett N., 2004, *MNRAS*, 348, 458
- Darwin G. H., 1879, *The Observatory*, 3, 79
- de Mink S. E., Langer N., Izzard R. G., Sana H., de Koter A., 2013, *ApJ*, 764, 166
- Dobbs-Dixon I., Lin D. N. C., Mardling R. A., 2004, *ApJ*, 610, 464
- Donati J.-F., Landstreet J. D., 2009, *ARA&A*, 47, 333
- Eggleton P. P., 1983, *ApJ*, 268, 368
- Eggleton P. P., Kiseleva L. G., Hut P., 1998, *ApJ*, 499, 853
- Goldreich P., Nicholson P. D., 1977, *Icarus*, 30, 301
- Heinz S., Sell P., Fender R. P., Jonker P. G., Brandt W. N., Calvelo-Santos D. E., Tzioumis A. K., Nowak M. A., Schulz N. S., Wijandans R., van der Klis M., 2013, *ApJ*, 779, 171
- Hurley J. R., Pols O. R., Tout C. A., 2000, *MNRAS*, 315, 543
- Hurley J. R., Tout C. A., Pols O. R., 2002, *MNRAS*, 329, 897
- Hut P., 1980, *A&A*, 92, 167
- Hut P., 1981, *A&A*, 99, 126
- Ivanov P. B., Papaloizou J. C. B., 2004, *MNRAS*, 353, 1161
- Ivanova N., Kalogera V., 2006, *ApJ*, 636, 985
- Ivanova N., Taam R. E., 2003, *ApJ*, 599, 516
- Jackson B., Greenberg R., Barnes R., 2008, *ApJ*, 678, 1396
- Janssen T., van Kerkwijk M. H., 2005, *A&A*, 439, 433
- Jonker P. G., Nelemans G., Bassa C. G., 2007, *MNRAS*, 374, 999
- Justham S., Rappaport S., Podsiadlowski P., 2006, *MNRAS*, 366, 1415
- Kalogera V., 1999, *ApJ*, 521, 723
- Kawaler S. D., 1988, *ApJ*, 333, 236
- Knigge C., Baraffe I., Patterson J., 2011, *ApJS*, 194, 28
- Lecar M., Wheeler J. C., McKee C. F., 1976, *ApJ*, 205, 556
- Ma B., Li X.-D., 2009, *ApJ*, 691, 1611
- Matsumura S., Peale S. J., Rasio F. A., 2010, *ApJ*, 725, 1995
- Nieuwenhuijzen H., de Jager C., 1990, *A&A*, 231, 134
- Ogilvie G. I., Lesur G., 2012, *MNRAS*, 422, 1975
- Ogilvie G. I., Lin D. N. C., 2007, *ApJ*, 661, 1180
- Orosz J. A., McClintock J. E., Aufdenberg J. P., Remillard R. A., Reid M. J., Narayan R., Gou L., 2011, *ApJ*, 742, 84
- Parker E. N., 1958, *ApJ*, 128, 677
- Parkinson P. M. S., Tournear D. M., Bloom E. D., Focke W. B., Reilly K. T., Wood K. S., Ray P. S., Wolff M. T., Scargle J. D., 2003, *ApJ*, 595, 333
- Penev K., Sasselov D., Robinson F., Demarque P., 2007, *ApJ*, 655, 1166
- Pols O. R., Schröder K.-P., Hurley J. R., Tout C. A., Eggleton P. P., 1998, *MNRAS*, 298, 525
- Portegies Zwart S., McMillan S., et al. H., 2009, *New A*, 14, 369
- Portegies Zwart S. F., Verbunt F., 1996, *A&A*, 309, 179
- Polyser E., Savonije G. J., 1988, *A&A*, 191, 57
- Rasio F. A., Tout C. A., Lubow S. H., Livio M., 1996, *ApJ*, 470, 1187
- Skumanich A., 1972, *ApJ*, 171, 565
- Tout C. A., Pols O. R., Eggleton P. P., Han Z., 1996, *MNRAS*, 281, 257
- Val Baker A. K. F., Norton A. J., Quaintrell H., 2005, *A&A*, 441, 685
- Valsecchi F., Rasio F. A., 2014, *ApJ*, 786, 102
- van der Meer A., Kaper L., van Kerkwijk M. H., van den Heuvel E. P. J., 2005, in Burderi L., Antonelli L. A., D'Antona F., di Salvo T., Israel G. L., Piersanti L., Tornambè A., Straniero O., eds, *Interacting Binaries: Accretion, Evolution, and Outcomes* Vol. 797 of American Institute of Physics Conference Series, On the mass distribution of neutron stars in HMXBs. pp 623–626
- van Kerkwijk M. H., van Paradijs J., Zuiderwijk E. J., 1995, *A&A*, 303, 497
- Verbunt F., Phinney E. S., 1995, *A&A*, 296, 709
- Verbunt F., Zwaan C., 1981, *A&A*, 100, L7
- Weber E. J., Davis Jr. L., 1967, *ApJ*, 148, 217
- Wong T.-W., Valsecchi F., Fragos T., Kalogera V., 2012, *ApJ*, 747, 111
- Yungelson L. R., Lasota J.-P., Nelemans G., Dubus G., van den Heuvel E. P. J., Dewi J., Portegies Zwart S., 2006, *A&A*, 454, 559
- Zahn J. P., 1966, *Annales d'Astrophysique*, 29, 489
- Zahn J.-P., 1975, *A&A*, 41, 329
- Zahn J.-P., 1977, *A&A*, 57, 383
- Zahn J.-P., 1989, *A&A*, 220, 112
- Zahn J.-P., 2008, in Goupil M.-J., Zahn J.-P., eds, *EAS Publications Series Vol. 29 of EAS Publications Series, Tidal dissipation in binary systems*. pp 67–90